JOINT EUROPEAN TORUS JET

JET–P(92)15

C.D. Challis, J.P. Christiansen, J.G. Cordey, C. Gormezano, C.W. Gowers,
G.J. Kramer, J. O'Rourke, P.M. Stubberfield, A. Taroni, F. Tibone,
B. Tubbing and JET Team

Current Ramp Experiments on the Scaling of Energy Confinement

Current Ramp Experiments on the Scaling of Energy Confinement

C.D. Challis, J.P. Christiansen, J.G. Cordey, C. Gormezano, C.W. Gowers,
G.J. Kramer[1], J. O'Rourke, P.M. Stubberfield, A. Taroni, F. Tibone,
B. Tubbing and JET Team*

JET-Joint Undertaking, Culham Science Centre, OX14 3DB, Abingdon, UK

[1]On attachment from FOM, Netherlands
** See Annex*

Preprint of Paper to be submitted for publication in
Nuclear Fusion

Current Ramp Experiments on the Scaling of Energy Confinement

C.D. Challis, J.P. Christiansen, J.G. Cordey, C. Gormezano, C.W. Gowers,
G.J. Kramer *, J. O'Rourke, P.M. Stubberfield, A. Taroni, F. Tibone, B. Tubbing

JET Joint Undertaking, Abingdon, Oxfordshire, OX14 3EA, England.
* On attachment from FOM, Netherlands

Abstract

The dependence of global and local confinement upon plasma current and poloidal field is studied in an analysis of JET data from a series of current ramp experiments. In such experiments the current profile is transiently decorrelated from its steady state shape over a period lasting more than ten confinement times. Global confinement is shown to depend not only on total current but also on some measure of the current distribution, e.g. the internal inductance. The origin of this dependence is found in the local analysis to be the dependence of diffusivity upon the poloidal field. A weak shear dependence of diffusivity is observed in the outer half of the plasma. Predictive transport calculations are made in which the electron-ion thermal diffusivities are based on a critical temperature gradient model; the calculations reproduce the measured temperature profiles to within the measurement errors. Simple mathematical expressions linking global to local confinement are used to demonstrate that the results from the global and local analysis are fully consistent.

1. Introduction

The dependence of global confinement properties in a Tokamak, the confinement time τ_E and stored plasma energy W, upon global plasma parameters, current I_ϕ, power P, average density n, has been well established empirically. A variety of scaling laws [1] has been derived and it has recently been shown that these laws are essentially all equivalent for L-mode plasmas to the ITER89P scaling law [2]

$$\tau_E = 0.048\ a^{0.3} R^{1.2} n^{0.1} I_\phi^{0.85} B_\phi^{0.2} P^{-0.5} \kappa^{0.5} A^{0.5} \qquad (1)$$

In Eq. (1) a, R, κ, A and B_ϕ refer to minor, major radius, plasma elongation, ion mass number and toroidal field; τ_E is the confinement time for total energy which includes that of fast ions.

In this paper the dependence of confinement on the plasma current I_ϕ is examined in greater detail from both a global and a local point of view. In particular it will be shown that the current profile shape also plays a role in the confinement as well as the

absolute value of the total current. A simple measure of the width of the current profile is the inductance ℓ_i. In steady state plasmas ℓ_i and I_ϕ are correlated, e.g. a large current is usually synonymous with low safety factor q, broad current profile and small value of ℓ_i. The current profile can be decorrelated from the total current by making a rapid current ramp either up or down. Such current ramp experiments have been carried out on TFTR [3], DIII-D, ASDEX [4], TUMAN-3 [5] and JET [6]. Section 2 describes the scenario adopted in the JET experiments. In the JET experiments the density n, the power P, the toroidal field B_ϕ, the elongation κ as well a, R, A have been kept constant and only the current I_ϕ is varied. The time evolution due to resistive diffusion of the current profile during the current ramp is studied in section 3. Calculations with the TRANSP code [7] are found to be consistent with JET diagnostic data such as that from loop volts, diamagnetic energy, polarimeter, soft X-rays. In section 4 it is shown that the global confinement time depends not only on I_ϕ as in Eq. (1) but also on ℓ_i. To examine the origin of the I_ϕ and ℓ_i dependence of τ_E we analyse in section 5 the time-space dependence of local confinement. The local diffusivity χ is inferred from calculations with the TRANSP code using measured profiles of the electron temperature T_e; χ is found to follow the evolution of the current profile.

The data from the JET current ramp experiments thus tells us that χ changes in response to changes in local parameters such as the poloidal field B_p, the safety factor q or the magnetic shear s. χ can therefore be described in terms of local parameters without the need to invoke "action at a distance" principles [8]. Indeed we show in section 5 that simple and dimensionally correct expressions for χ can adequately describe the data.

In section 6 the data is compared with results from predictive calculations with the JETTO code [9]. The transport model of Rebut, Lallia, Watkins [10] can predict the measured global confinement time and the difference between measured and predicted temperature profiles are within the experimental error bars.

In section 7 we summarize the results presented in this paper and discuss some implications for global confinement scaling and local transport models.

2. Current ramp experiments

The experimental scenario adopted for JET is indicated schematically in Figure 1. This Figure shows the plasma current I_ϕ (t) for four types of pulses: two reference pulses at a steady 1.5 and 3 MA respectively and two pulses in which I_ϕ is either ramped up from 1.5 to 3 MA or ramped down from 3 to 1.5 MA; in both pulses the ramp time is 2 sec. The ramp up of I_ϕ is produced by changing the surface voltage V_ϕ as indicated by two

solid curves in Figure 2. The current ramp takes place during an 8 sec ICRF heating pulse at a constant level of 8 MW. Optimum programming of the poloidal field coil currents maintains nearly constant plasma shape during the ramp. Consequently the plasma density and Z_{eff} are approximately constant during 4 ramp-up, 4 ramp-down and 2 reference pulses.

The ramping (up-or-down) of the current arises from changes to the electric field $\underline{E}$ at the plasma edge. The changes to $\underline{E}$ and $\underline{B}$ propagate inwards from the edge due to resistive diffusion. During the ramp and for some period after the end of the ramp the spatial profiles of B_p, q and s will evolve towards a new steady state. In the TRANSP calculations Ohm's law and Maxwell's equations are solved with a neoclassical resistivity profile determined from the measured T_e profiles. In the JETTO calculations the neoclassical resistivity is determined from the predicted T_e profiles. Both sets of calculations employ the same definitions of q, s, ℓ_i; letting x denote a dimensionless flux surface label ($0 \le x \le 1$) we have

$$q(x) = \frac{RB_\phi}{2\pi}\int \frac{d\ell}{R^2 B_p} \quad , \quad s(x) = \frac{1}{q}\frac{dq}{dx} \quad , \quad \ell_i = \frac{4}{\mu_o R_o I_\phi{}^2}\int \frac{B_p{}^2}{2\mu_o}\, dv \qquad (2)$$

where R_o is the magnetic axis.

Relevant parameters for the JET current ramp experiments are summarized in Table I together with the corresponding values from TFTR and DIII-D. It can be seen that the ratio $\tau_{RAMP}/\tau_\eta \sim 0.5$ in all 3 Tokamaks although this ratio has been made smaller in some TFTR experiments. τ_{RAMP} is the current ramp time and τ_η represents a measure of the resistive diffusion time $\tau_\eta = C\, a^2\, T_{eo}^{3/2}$; C is a constant determined by matching τ_η to the time at which a steady state has been reached.

3. Evolution of current distribution

The inferences drawn about the role of the current distribution in confinement are based upon field diffusion calculations with the TRANSP code [7]. It is therefore important to verify that the results from such calculations are consistent with available diagnostic data. The curves in Figure 2 representing the calculated surface voltage V_ϕ (dashed curves) for the ramp up-down pulses agree very well with the measured V_ϕ ones (solid curves). Figure 3 shows for the same two pulses the evolution of the internal inductance ℓ_i; the full curves are based on MHD fits by the IDENTD code [11] and the dashed curves are from TRANSP. From the time evolution of ℓ_i in Figure 3 we notice that a steady state, i.e. $\nabla \times \underline{E} = 0$, is approached faster for a ramp-up pulse than

for a ramp down pulse; the ramp up pulse has initially a lower T_e and hence higher resistivity in the outside region than the ramp down pulse.

All pulses considered are sawtoothing throughout the ICRF heating phase; Figure 4 shows the agreement between the positions of the q = 1 inversion surfaces derived from soft x-ray tomography and that predicted by TRANSP from a Kadomtsev model. The most direct measure on JET of the current distribution is provided by polarimetric data. From Abel-inverted q profiles we have extracted q (t) at the radial positions R = 3.5, 3.75 and 4 m. Figures 5a (ramp down pulse) and 5b (ramp up pulse) both show that the solid lines representing q(t) from polarimetric data compare well with the dashed curves obtained from TRANSP.
We thus conclude that the TRANSP calculations represent a good description of local resistive diffusion in the current ramp experiments. The role of the current distribution in confinement can therefore be assessed from the TRANSP results (section 5).

4. Global confinement

The total stored plasma energy W is estimated from JET data in several ways: [i] W_{MHD} from MHD fits, [ii] W_{dia} from diamagnetic measurements, [iii] W_{kin} from interferometer data, ECE profile data, X-ray crystal spectrometer data and visible bremsstrahlung data ($W = W_e + W_i$). All three estimates of W are found to be consistent with each other when the energy content of the fast minority ions (ICRH) is taken into account. This energy content has been evaluated by a reduced-order full-wave code SPRUCE [12] which is part of TRANSP.

In Figure 6 we show the time variation of W_{MHD} for the same 4 pulses used in Figure 1. The two dashed lines in Figure 6 representing the 1.5 and 3 MA steady state pulses demonstrate the impact of current scaling in steady state. The evolutions of W for the current ramp pulses show that W eventually approaches the steady state values some 4-5 seconds (or 10-20 confinement times) after the end of the ramp. The global confinement at constant power, density and plasma shape does therefore <u>not</u> depend on the current I_ϕ alone, but also on the current distribution.

We have combined data from the 10 JET pulses which all have P(ICRH) = 8 MW with data from 4 pulses which have P(ICRH) = 5 MW; in these 4 pulses from 1990 [6] the current has been ramped up from 2 to 3 MA and down from 3 to 2 MA. The combined data is separated into two groups as follows: [i] steady state data includes that of the two reference pulses plus data up to t = 48 sec. when the ramp starts; [ii] non-steady state data includes that after t = 48 sec for the ramp pulses. Because several of the global

parameters of Eq. (1) remain fixed in the JET experiments we can fit the data of two groups to the following expressions (ss ~ steady state, ns ~ non steady state)

$$W_{ss} = C_{ss}\ n^{z_n}\ I_\phi^{z_I}\ P^{z_P} \qquad (3a)$$

$$W_{ns} = C_{ns}\ n^{z_n}\ I_\phi^{z_I}\ P^{z_P}\ \ell_i^{z_\ell} \qquad (3b)$$

The values of the constants C_{ss} and the exponents z_n, z_I etc. are given in Table II together with the r.m.s. error. The steady state data can be well represented by either W_{ss} or W_{ns}. The non-steady state data can however not be represented by W_{ss}. Plots of fits of all the data to Eqs. (3a) and (3b) are shown respectively in Figures 7a and 7b. The best fit (Figure 7b) can be approximated by

$$W \sim I_\phi^{4/3}\ \ell_i^{2/3} \qquad (4)$$

Global confinement thus depends on the current distribution; a measure of the latter, such as ℓ_i, should hence be included in scaling law expressions like Eq. (1). The analysis and the result just described apply to the data on W_{MHD}. The same analysis has been performed on the data of W_{dia} and W_{kin} and the same scaling expressed by (4) is established but with different values for the coefficients in z_n, z_p because of the contribution from the fast ion energy content.

5. Local transport. Interpretative analysis

From the evolution of the measured T_e profiles TRANSP evaluates an effective diffusivity defined as

$$\chi = \frac{P(x)}{eV' \langle |\nabla x|^2 \rangle \left(n_e T_e' + n_i T_i' \right)} \qquad (5)$$

V and P(x) are the total volume and power inside a flux surface x and the prime denotes a derivative w.r.t. x. In the current ramp experiments insufficient ion temperature data is available to permit an evaluation of χ_i and χ_e separately. In the TRANSP calculations the T_i profile is calculated by assuming that χ_i is proportional the neoclassical value; the constant of proportionality is fixed by matching the axial value T_{io} to data from the X-ray crystal spectrometer. At t = 9.6s the calculated T_i profile agrees well with the only T_i profile available from charge exchange spectroscopy. The estimate of χ given by Eq. (5) has associated error bars which are discussed in more detail in [13]. In the central region the uncertainties arise from the sawtooth model used (Kadomtsev) as well as from the ICRH deposition model. In the outside region

the uncertainties on χ increase because the measurement errors on n_e and T_e and thus ∇T_e all increase.

In order to demonstrate how changes to the plasma profiles propagate inwards from the edge by resistive diffusion we show in Figures 8 and 9 $\Delta B_p/(\Delta B_p)$ max and $\Delta\chi/(\Delta\chi)$ max; $\Delta B_p = B_p(t) - B_p(t = 8s)$ and similarly for χ. These ratios shown for x = 0.55, 0.65, 0.75 in Figures 8 and 9, start from 0 at the onset of the current ramp and approach + 1 or -1 as a new steady state is reached. From Figure 8 we can see that the current diffusion proceeds faster for the ramp up pulse than it does for the ramp down pulse. The difference is due to the difference in the T_e profiles at t = 8 seconds. For both pulses the evolution of B_p at x = 0.75 is lagging that at x = 0.55 by approximately 2 seconds. Figure 9 emphasizes in a similar way how the changes to χ proceed at a faster rate for the ramp up pulse than for the ramp down pulse. For the latter pulse Figure 9 shows clearly how χ at x = 0.75 responds some 2 seconds before a change occurs at x = 0.55; we also notice that $\Delta\chi \leq 0$ during the ramp down period. The time evolution of χ as illustrated by the changes of Figure 9 emphasizes that the "TRANSP data" on χ can be described in terms of local values of the plasma profiles for T, n, B_p, q, s etc.

Since the JET current ramp experiments have been carried out at constant density and power we are unable to determine the n and T dependence of χ; data from different experiments in which the current is ramped at other constant levels of P and n would be required. This limitation restricts us to consider only simple, but dimensionally correct expressions for χ. We have chosen to represent χ at each radius x by

$$\chi_{\text{model}} = \chi_o C_\chi s^\mu q_\psi^\lambda \qquad (6)$$

A fit of the data on χ to χ_{model} serves to determine the dimensionless parameters C_χ, μ and λ at each radius. The diffusivity χ_o is chosen as either the Bohm or gyro-Bohm forms

$$\chi_o = \chi_B = \frac{T_e}{B_p} \quad , \quad \chi_o = \chi_{GB} = \chi_B \rho_* = \chi_B \left(\frac{m_e T_e}{e a^2 B_p^2} \right)^{1/2} \qquad (7)$$

Both scalings Eq. (7) result approximately in the experimentally observed I_ϕ and P dependence of τ_E in steady state.

The result of the data fitting is illustrated in Figure 10 which shows the variations with x of the exponents μ of Eq. (6) for both scalings (7). The variation with x of the normalising constant C_χ (not shown) exhibits the "bowl shape", characteristic of L-mode confinement profiles for χ. This variation is not described by the data from the

ramp experiments as already explained and it may involve some additional dependencies of χ upon T_e, T_i, n etc. We notice however from Figure 10 that both the Bohm and gyro-Bohm scalings, when assumed, imply some shear dependence, weaker in the centre where the shear is low and stronger in the outside region. However, the major changes to χ as shown in Figure 9 arise from those of the local poloidal field B_p. Since $q_\psi = \varepsilon B_\phi / B_p$ we see from Eqs. (6 - 7) and Figure 10 that the overall scaling of χ with B_p becomes

$$\chi \sim B_p^y \quad , \quad -1.7 < y < -1.3 \tag{8}$$

6. Local transport. Predictive calculations

As a further test of the local nature of the energy transport in these experiments, simulations have been carried out by means of the predictive $1\frac{1}{2}$ D transport code JETTO [9]. Only the evolutions of temperature and current density profiles have been computed. The evolution of density profiles has been taken from the experimental results. The transport model used is the Rebut-Lallia-Watkins model [10] for the electron heat flux, with the assumption of equal electron and ion thermal conductivities. Neoclassical resistivity has been assumed as in the interpretative analysis.

The results of the simulations of both global and local quantities, including the magnetic ones, are compatible with the experimental observations both for the current ramp down and ramp up experiments. As an example of the results obtained, fig. 11 compares the computed and the experimental time evolution of the thermal electron energy content in the case of a current ramp down pulse. For the same discharge fig. 12 compares the experimental (ECE) and computed electron temperature profiles in the middle and at the end of the current ramp. Fig. 13 shows the time evolution of the total heat flux $Q = V'q$ at $x = 0.8$ calculated for the ramp down pulse as follows: the solid curve is Q(t) calculated from the expression for χ_e using experimental profile data; the dot-dashed curve is Q(t) predicted by the JETTO code while the dashed curve represents the experimentally determined Q(t). We see from Figures 12 and 13 that the predicted Q can match the experimental Q via slight changes to the T_e profiles. Because the model of [10] is strongly non-linear i.e.

$$q_{model} \sim -en\ \chi\left(\nabla T - (\nabla T)_{crit}\right) \quad ,$$

any slight change to T_e (Figures 12a and 12b) yields a large change to q and Q. This explains the significant discrepancy between the solid and dashed curves of Figure 13. The predictive calculations do therefore not validate the complete prescription for

q_{model}, the main ingredient of the model which has been tested is the dependence $\chi \sim q_\psi/s$ which is found to be compatible with the results from the interpretative analysis of section 5.

7. Interpretation and implications of results

The JET current ramp experiments have produced data in which all the parameters, except I_ϕ, entering the ITER89P scaling law (Eq. 1) are held approximately constant. In this data the values of I_ϕ are decorrelated from those of ℓ_i on a timescale $\tau_\eta >> \tau_E$ (see Table I). The analysis demonstrates that τ_E depends on both the total plasma current I_ϕ and its distribution J_ϕ; the best characterization of the global data is expressed by Eq. (4) i.e. in terms of I_ϕ and ℓ_i. The local transport analysis shows that the origin of the ℓ_i scaling is the dependence of the effective diffusivity χ upon the local poloidal field B_p. The results from the local and global analyses are thus fully consistent and this can be explained by the following simple argument. From the study of Callen et al. [14] the global confinement time τ_E can be calculated as

$$\tau_E = \frac{W_1}{P} + \frac{1}{P}\int_o^1 \frac{3}{2} N(x) \frac{P(x)\,dx}{n(x)V' < |\nabla x|^2 > \chi} \qquad (9)$$

where $W_1 = \frac{3}{2}$ e N(x = 1 T(x = 1) and N(x) is the total particle inventory up to radius x with n(x) = n_e(x) + n_i(x). It is obvious that χ must include some dependence upon n and T for (9) to explain the experimental scalings, e.g. $n^{0.2}$ $P^{-0.5}$ (say). As already emphasized, the present data does not describe the n and T scalings of χ. It is however evident from Eq. (9) that since the local analysis shows $\chi \sim B_p{}^y$ (Eq. 8) then τ_E must depend on some integral of B_p. With a simple model of constant n, P(x) = P_o δ(x) and χ independent on n and T Eq. (9) gives $\tau_E \sim h_i I_\phi$ or $\ell_i I_\phi{}^2$ for y = - 1 or -2 respectively (h_i is flux inductance); some more complex model with $\chi = \chi$ (n, T, B_p, ...) will not only produce the experimentally observed n and P scaling but it will also yield the scaling of Eq. (4) which is somewhere between the limits y = - 1 and - 2 mentioned above.

The results obtained from our analysis show that theoretical models which predict a scaling $\chi \sim B_p{}^y s^\mu$ with $-2 \le y \le -1$, $-1 < \mu < o$, are compatible with the data; one such model with y = -2, μ = -1 [10] has been tested against the data. The implication of this χ scaling is that scaling expressions for τ_E should therefore in general explicitly include some measure of the current distribution, e.g. the plasma internal inductance ℓ_i.

Acknowledgements

The authors acknowledge the work of the JET team for carrying out these experiments.

Parameter	DIII-D	TFTR	JET
τ_E (sec) at 1	0.04	0.07	0.2
τ_{RAMP} (sec, 1 → 21)	0.1-	0.2-1	2
τ_η ($a^2T^{3/2}$, sec)	0.2-0.25	1.3-1.7	4-5
Heating period τ_{HEAT} (sec)	0.5	2	8
Power (MW)	15 NBI	11 NBI	8 ICRH
Current 1 (MA)	0.4	1	1.5
Elongation κ	1+	1	1.3
q_ψ or q_{95}	6	6	7
n_e ($10^{19}m^{-3}$)	5	3.4-8.1	2.5
T_e (keV)	2.3	5	8

Table I. Relevant parameters for current ramp experiments on DIII-D, TFTR and JET.

	C	Z_n	Z_I	Z_P	Z_e	σ
Steady state	0.56	0.16	0.71	0.43	-	11.5
Non-steady state	0.30	0.14	1.31	0.36	0.68	6.5

Table II. Values of the exponents and constants in Eqs. (4-5). The units used are W(MJ), n($10^{19}m^{-3}$) P(MW). σ denotes the r.m.s. error in % from the fit.

References

[1] GOLDSTON, R.J., Plasma Phys. Contr. Fusion 26 (1984) 87
KAYE, S.M., GOLDSTON, R.J., Nucl. Fusion 25 (1985) 65
STRELKOV, V.S., Nucl. Fusion 25 (1985) 1189
GRUBER, O., in Plasma Physics (Proc. Int. Conf. Lausanne 1984), vol. 1, CEC, Brussels (1984) 67
SHIMOMURA, Y., Empirical scaling of Energy Confinement of L-mode plasma and optimized mode and some consideration of Reactor Core Plasma in Tokamak, Rep. IAERI-M 87-080, Japan Atomic Energy Research Institute, Ibaraki (1987).

[2] YUSHMANOV, P.N., TAKIZUKA, T., RIEDEL, K.S., et al., Nucl. Fusion 30 (1990) 1999.

[3] ZARNSTORFF, M.C. and the TFTR group, Analysis of TFTR current profile perturbation experiments, TTF Workshop, Austin, Texas, 19th March 1991.

[4] MURMAN, H., STROTH, U., in Controlled Fusion and Plasma Physics (Proc. 18th Eur. Conf. Berlin, 1991), Vol. 15C, Part I, European Physical Society (1991) 109.

[5] ASKINASI, L.G., AFANASIEV, V.I., GOLANT, V.E. et al, ibid, p. 149.

[6] O'ROURKE, J., BALET, B., CHALLIS, C., et al., ibid, p.37.

[7] HAWRYLUK, R.J., An empirical approach to Tokamak Transport, Proc. Course and Workshop 1979 p.19, Varenna (1980).
GOLDSTON, R.J., J. Comp. Phys. 43 (1981) 61.

[8] HAWRYLUK, R.J., ARUNASALAM, V., BARNES, C.W. et al, Plasma Physics and Controlled Fusion, 33 (1991) 1509.

[9] ENACCHI, G., TARONI, A., JETTO: A-free boundary plasma transport code (basic version), JET internal Report JET-IR(88) 03, 1988.

[10] REBUT, P.H., LALLIA, P.P., WATKINS, M.L., in Plasma Physics and Controlled Nuclear Fusion Research, 1988 (Proc. 12th Int. Conf. Nice, 1988) Vol. 2, IAEA, Vienna (1991) 191.

[11] BLUM, J., LEFOLL, J., J. Comput. Phys. Rep. 1 (1984) 465.

[12] SMITHE, D.N. et al. Nucl. Fusion 27 (1987) 1319.

[13] BALET, B., BOYD, D.A., CAMPBELL, D.J. et al., Nucl. Fusion 30 (1990) 2029.

[14] CALLEN, J.D., CHRISTIANSEN, J.P., CORDEY, J.G., THOMAS, P.R., THOMSEN, K., Nucl. Fusion 27 (1987) 1857.

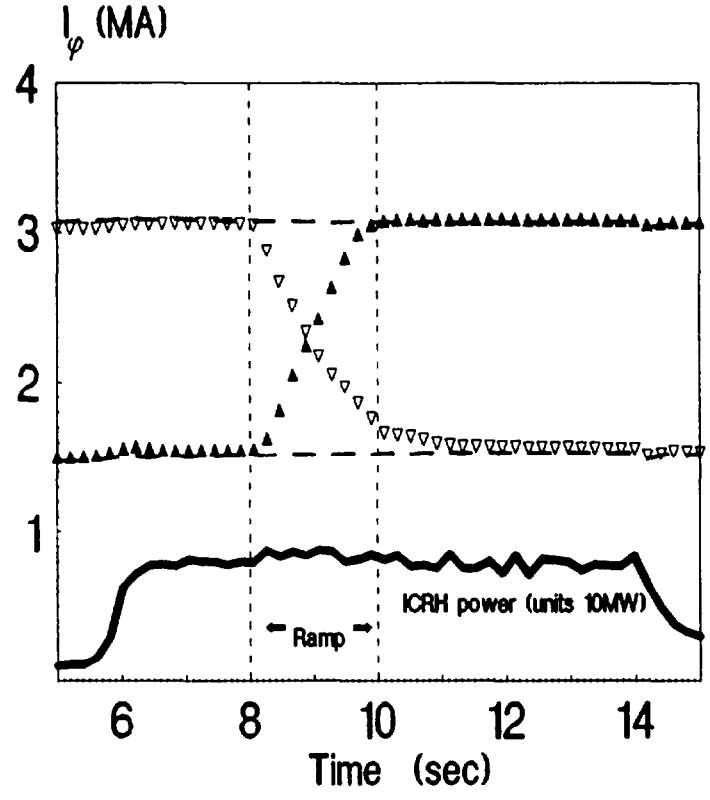

Figure 1. Plasma current I_ϕ in JET current ramp scenarios at constant ICRH power of 8 MW. The two dashed curves are for reference pulses #25360 and #25367. The solid curves plus triangles pointing down-up are for the ramp down-up pulses #25350 and #25365 respectively.

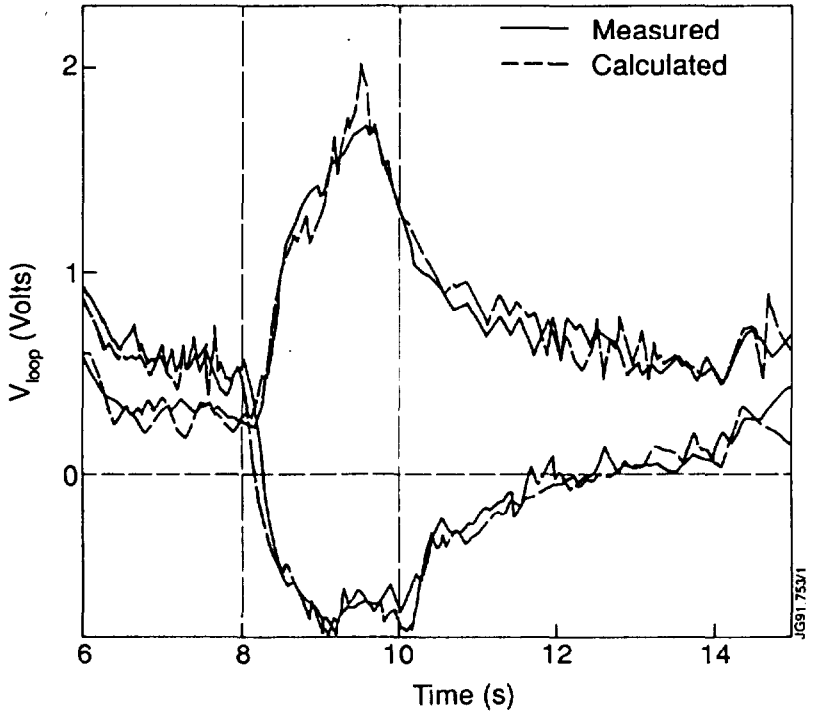

Figure 2. Evolution of loop voltage V_ϕ at the plasma edge for ramp down-up pulses from TRANSP calculations (dashed curves) follows the measured values (solid curves).

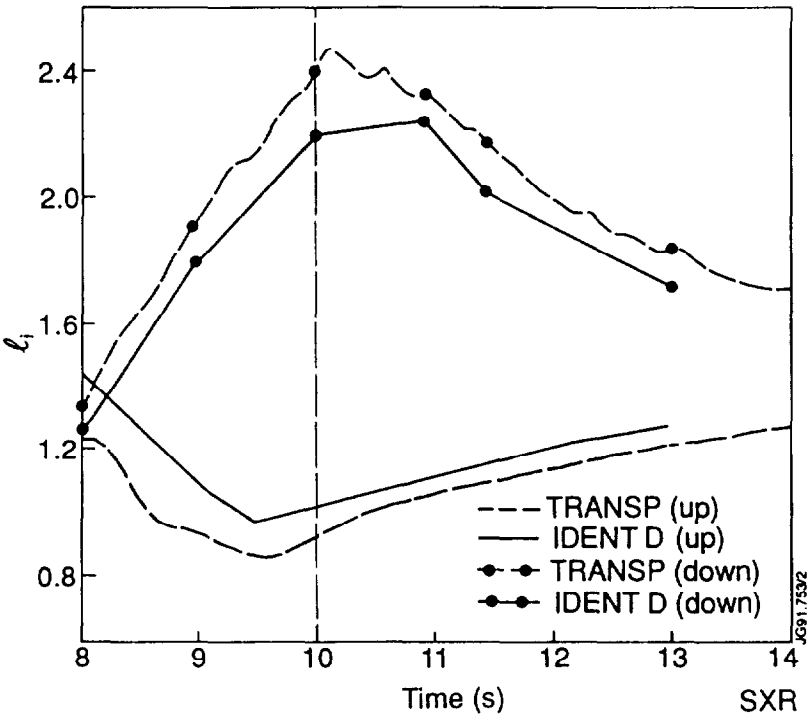

Figure 3. The internal inductant ℓ_i from TRANSP calculations (dashed curves) agrees with that determined in Equilibrium identifications which use magnetic and polarimeter data (solid curves).

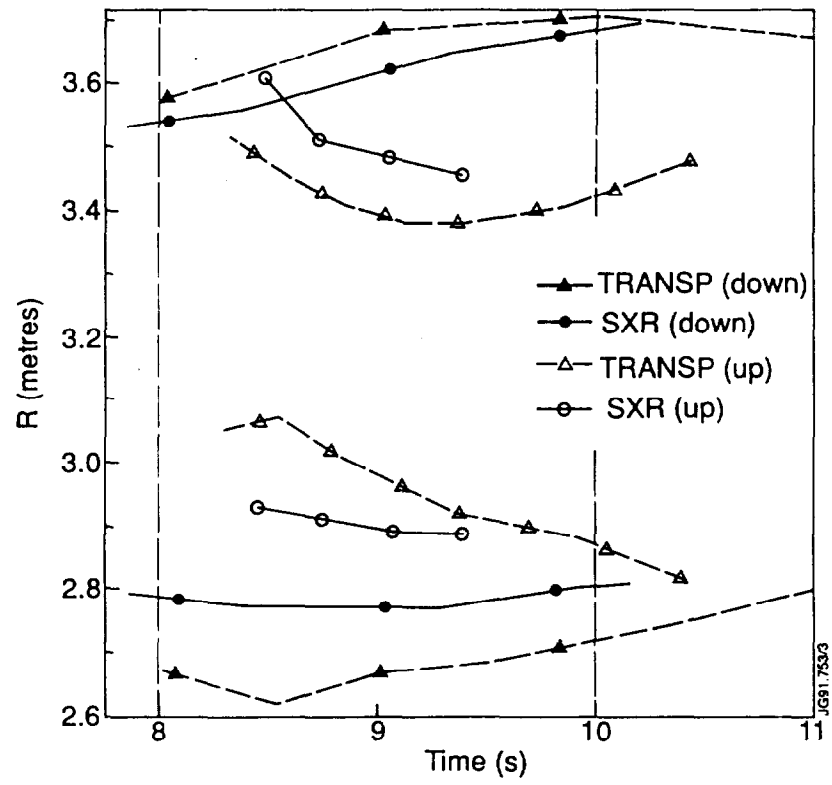

Figure 4. The midplane radial positions of the q = 1 surfaces evaluated by TRANSP (dashed curves) evolve similarly to those derived from tomography of soft X-ray data (solid curves).

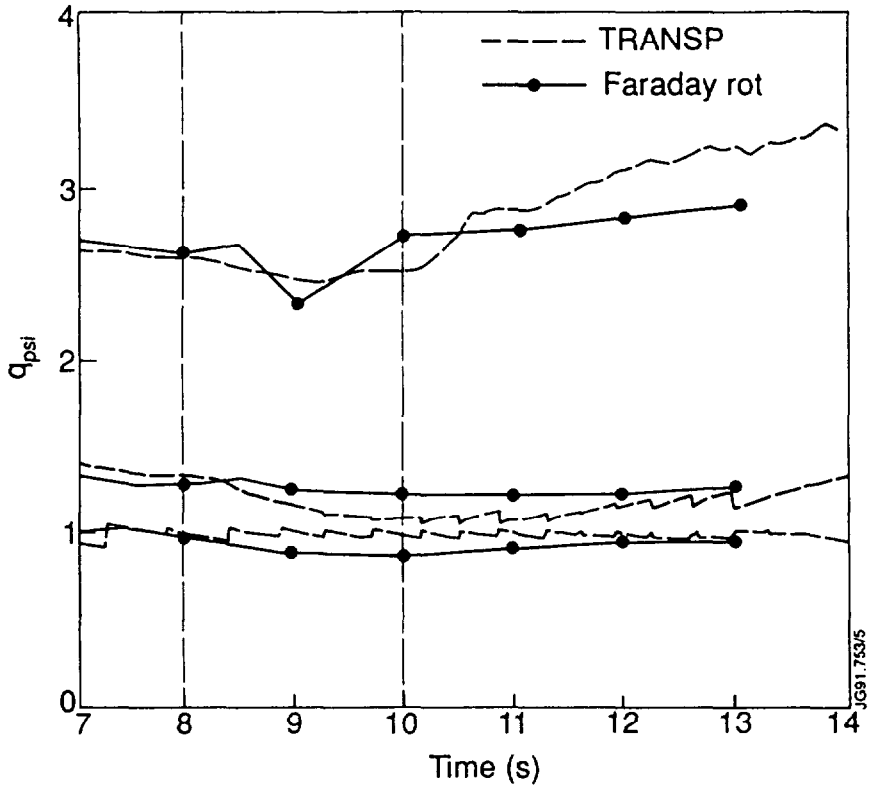

Figure 5a. Comparison between TRANSP values (dashed curves) and results from Abel inversion of polarimeter data (solid curves). The safety factor at three radii R = 3.5, 3.75, 4m is shown as a function of time for the ramp down pulse #25350.

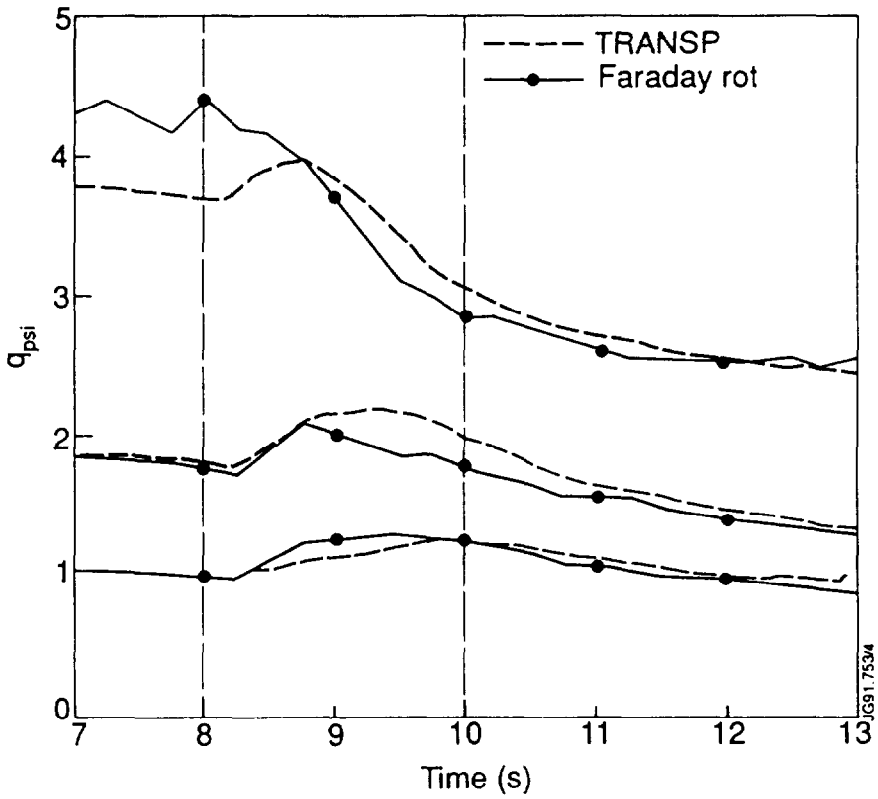

Figure 5b. As Figure 5a but for the ramp up pulse #25365.

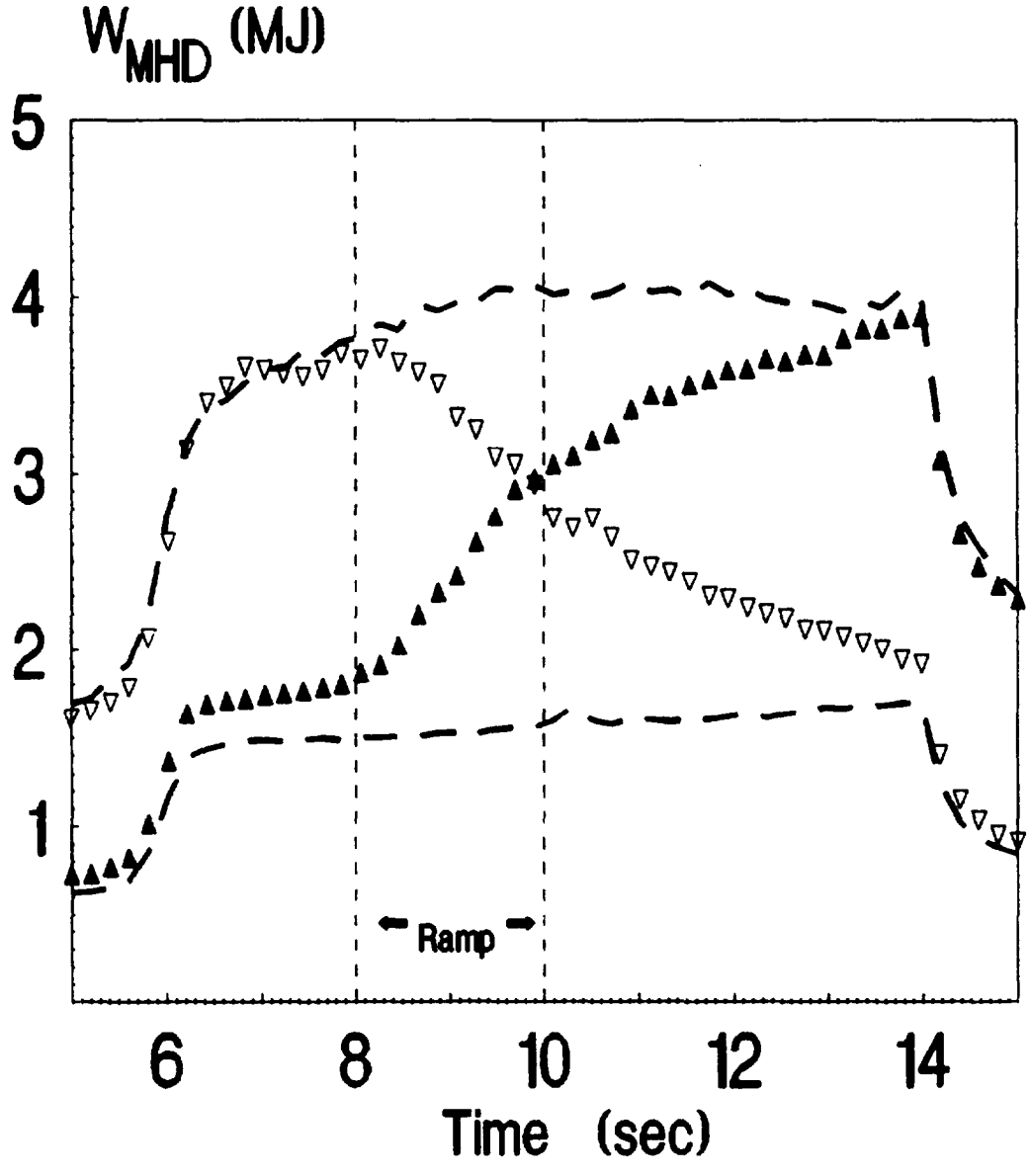

Figure 6. Changes to the total stored energy W_{MHD} determined from MHD fits. Legend as for Figure 1.

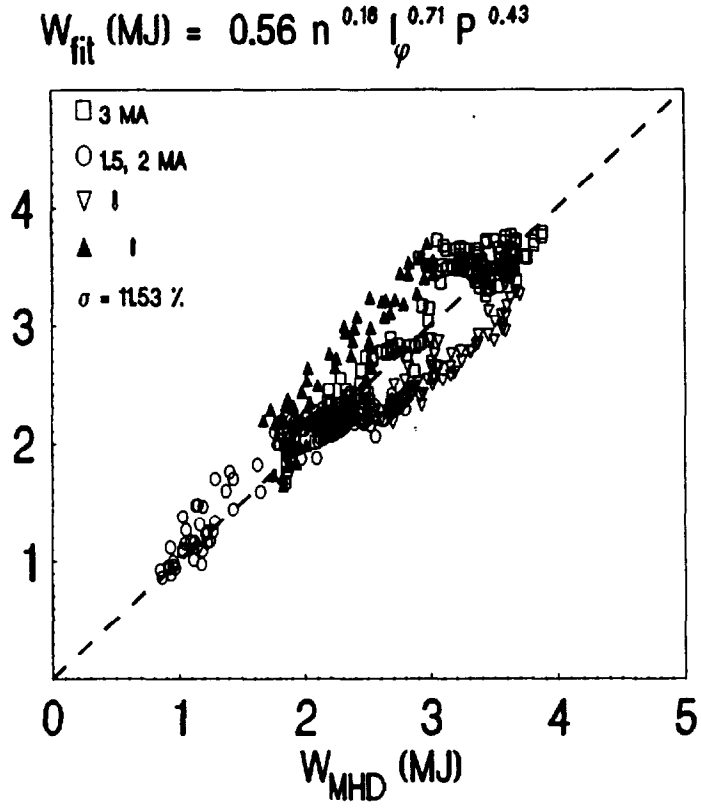

Figure 7a. Values fitted to W_{ss} (Eq. 4) do not match those of W_{MHD}. The units of the fitted expression are P(MW), I_ϕ(MA), n(10^{19} m^{-3}).

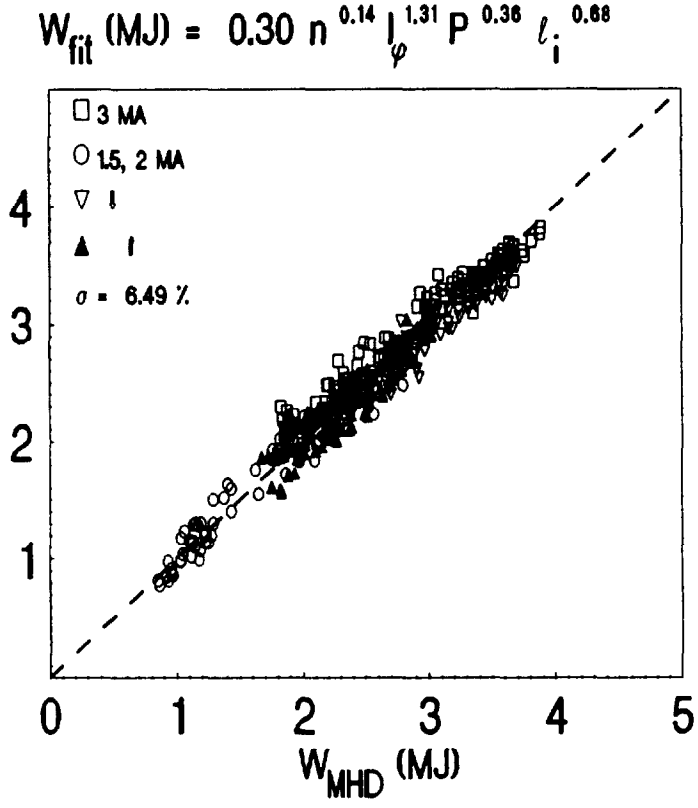

Figure 7b. The fit to W_{ns} (Eq. 5) of W_{MHD} shows that ℓ_i needs to be included as an independent variable. Thereby the r.m.s. error σ is halved (compare with Figure 7a).

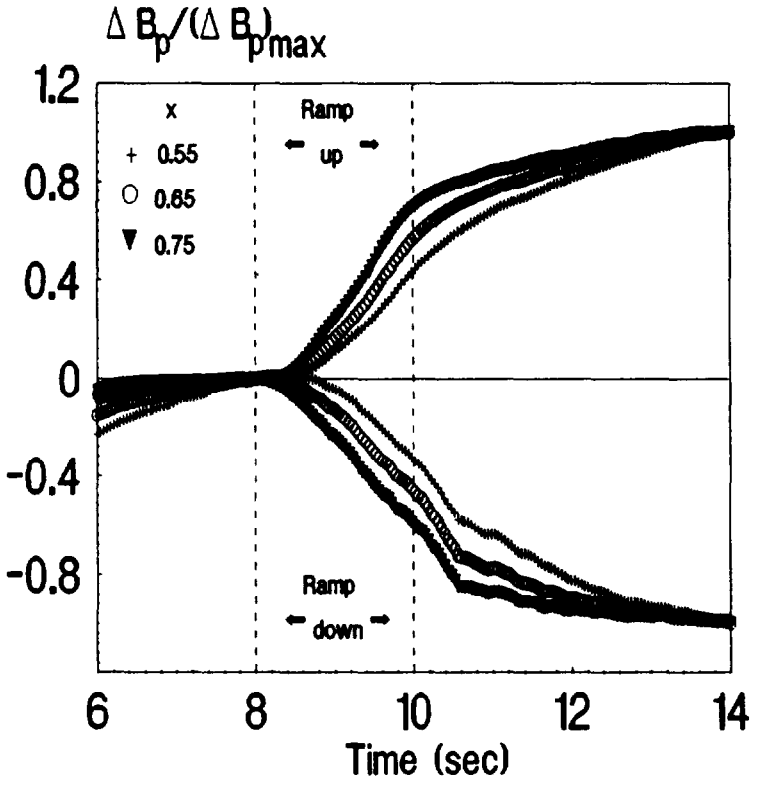

Figure 8. The changes to the poloidal field at x = 0.55, 0.65 and 0.75 for the ramp-up-down pulses are shown as the ratio $\Delta B_p/(\Delta B_p)$max vs time. $\Delta B_p = B_p(t) - B_p(t = 8s)$.

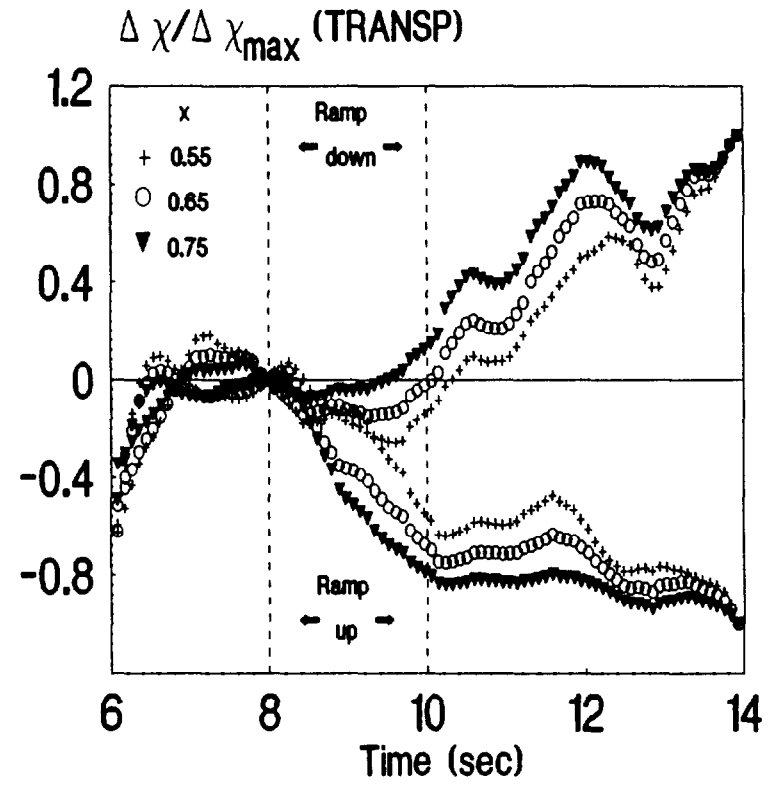

Figure 9. The responses in the diffusivity χ (Eq. 5) due to changes in B_p are illustrated by the time evolution of the ratio $\Delta\chi/(\Delta\chi)$max. $\Delta\chi = \chi(t) - \chi(t = 8s)$. Notice the difference between the ramp up and down pulses.

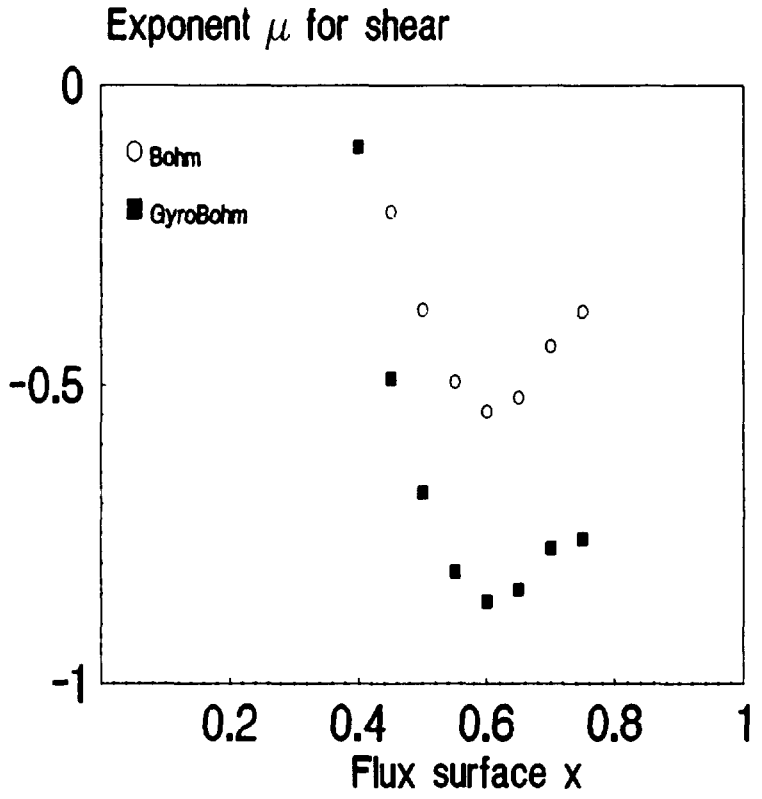

Figure 10. The dependence of χ upon shear is shown as the spatial variation of the exponent μ (Eq. 6).

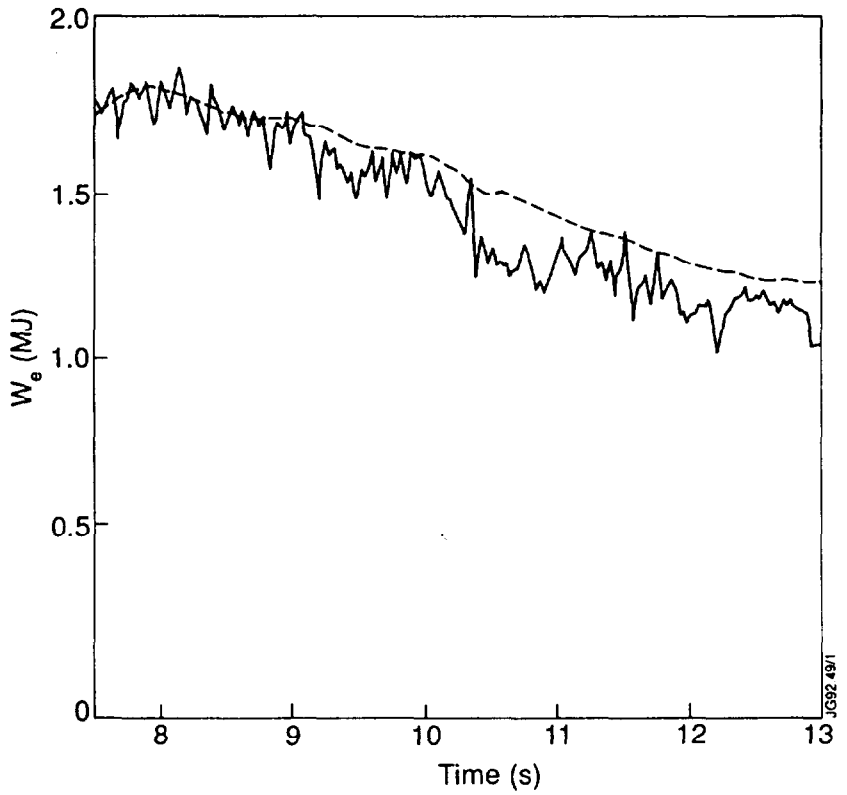

Figure 11. Time variation of electron thermal energy W_e. The solid line represents measurements and the dashed line refers to values predicted by the JETTO code.

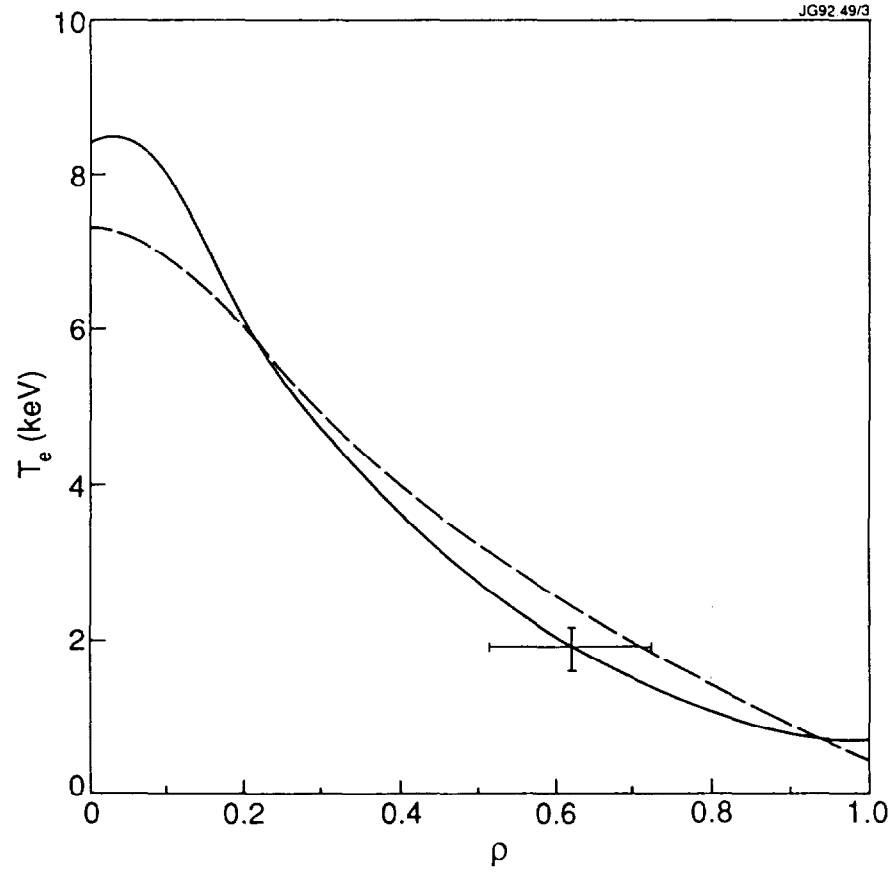

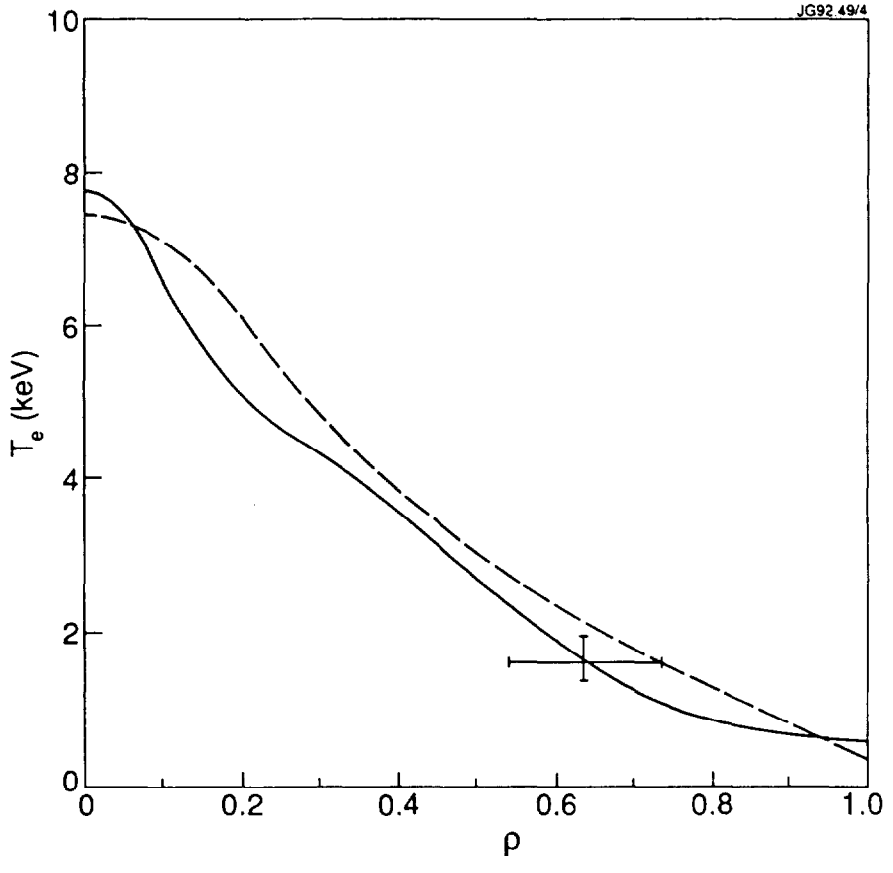

Figure 12. Measured (solid curve) and predicted (JETTO, dashed curve) T_e profiles for the ramp-down pulse #25350 at (a) 9s. and (b) 10s. $\rho = x$ (see text).

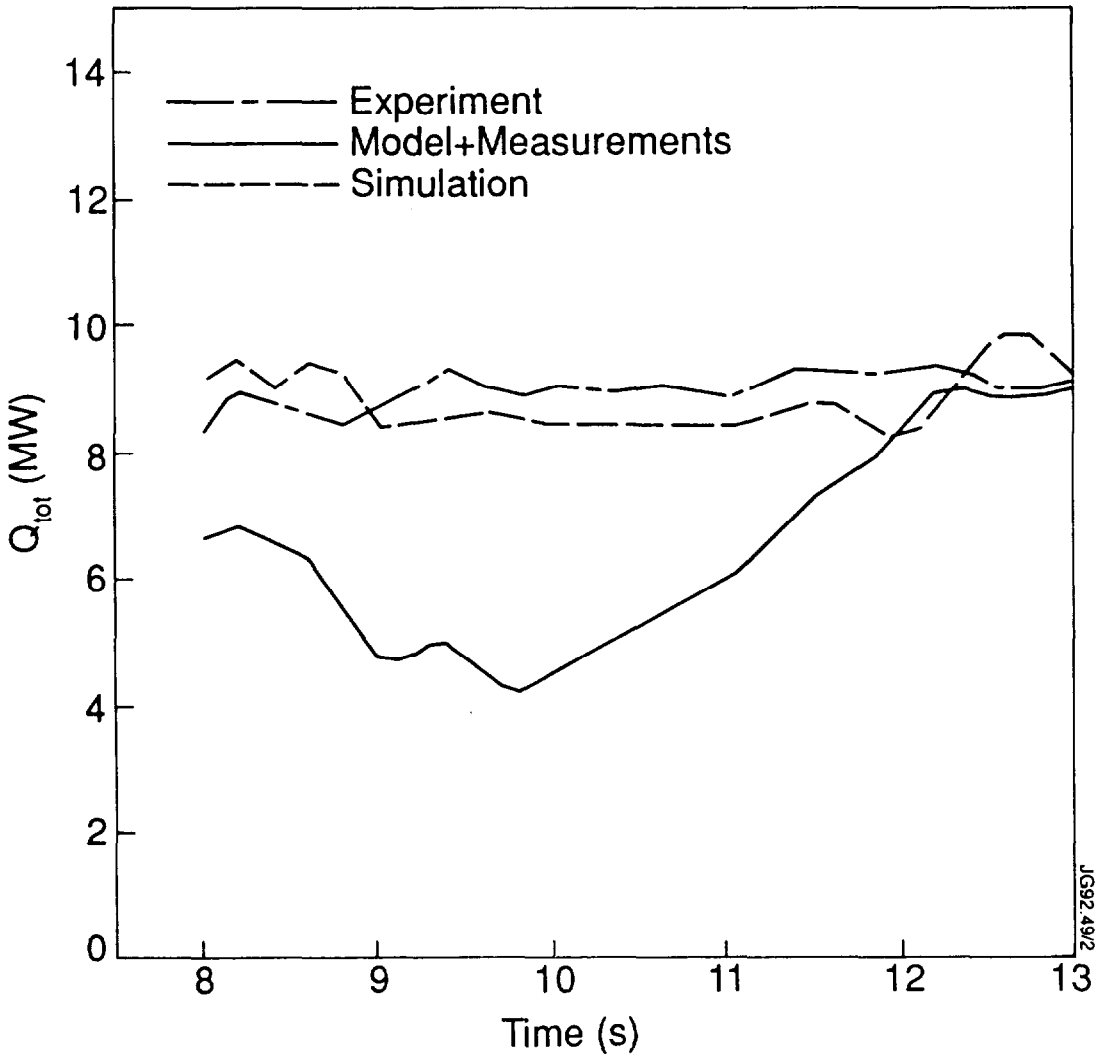

Figure 13. The total heat flow Q at x = 0.8 vs time. Solid curve: Q calculated from the expression for χ_e of [10] using experimental T_e profiles (solid curves of Figure 12). Dashed curve: Q predicted by the JETTO code corresponds to the predicted T_e profiles (dashed curves of Figure 12). Dot-dashed curve the experimental Q.

66
FIG 9

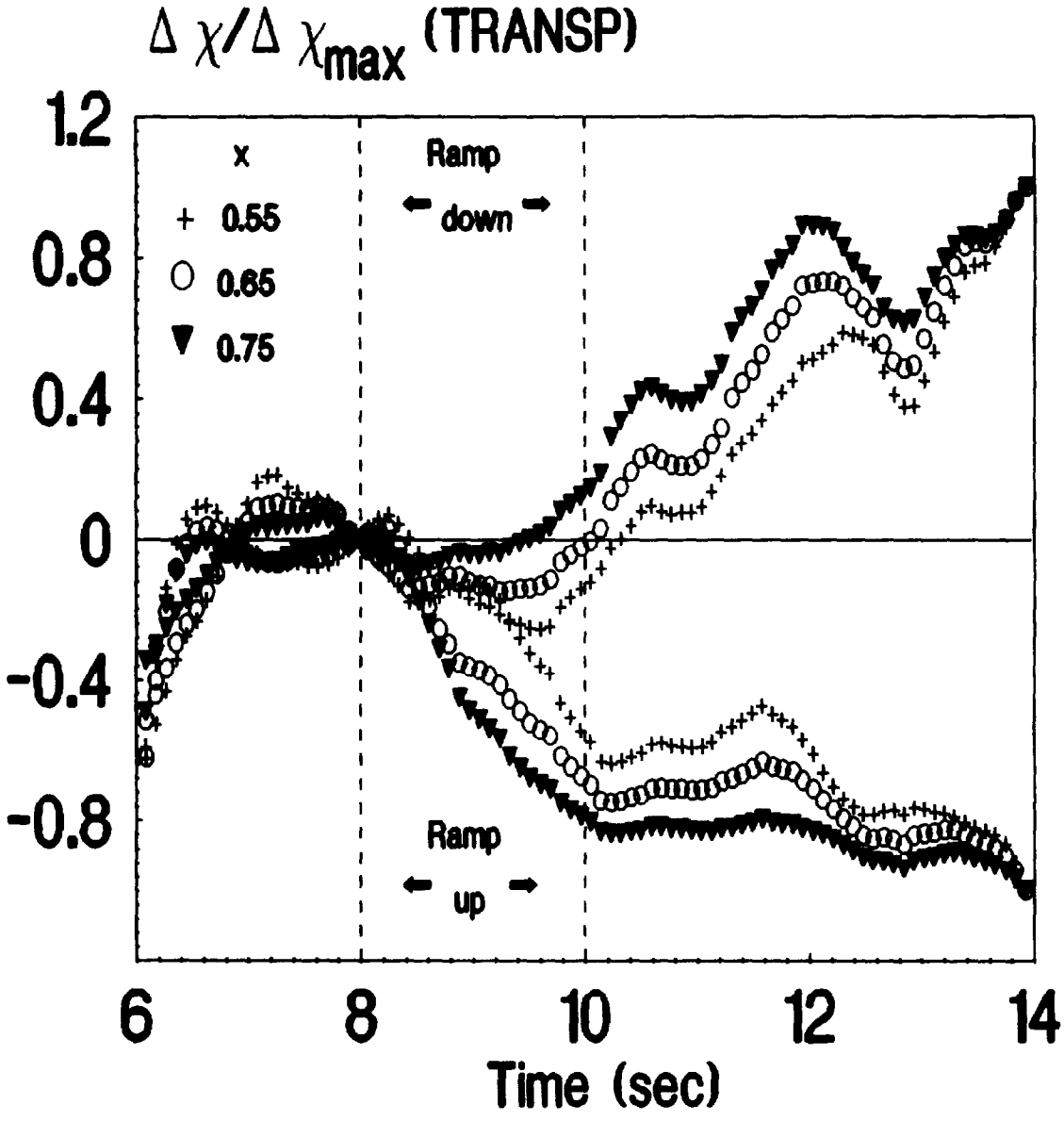
Δ χ/Δ χmax (TRANSP)
1.2
0.8
0.4
0
-0.4
-0.8
x
+ 0.55
O 0.65
▼ 0.75
Ramp
down
Ramp
up
6
8
10
12
14
Time (sec)

FIG 8

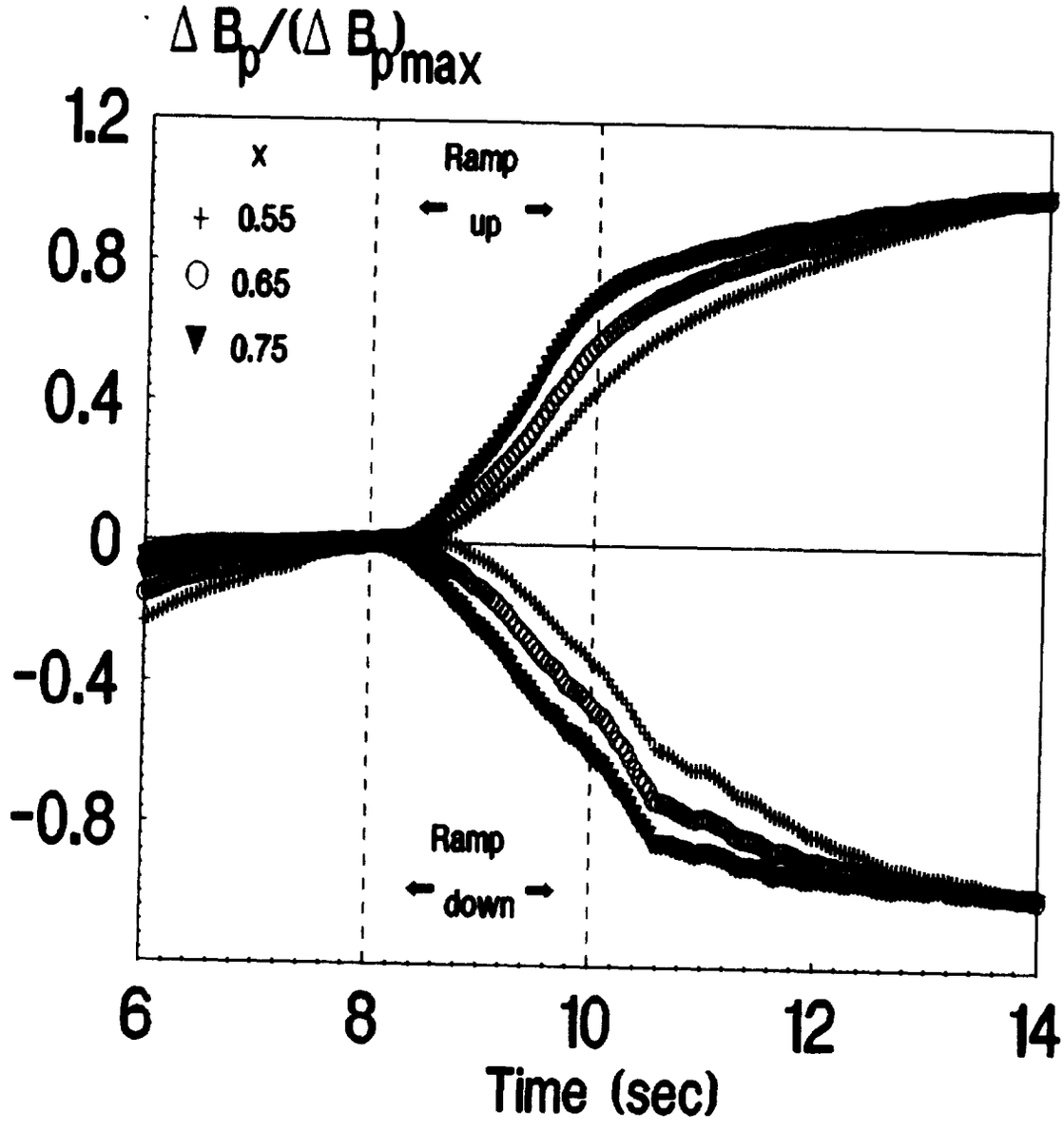
$\Delta B_p/(\Delta B_p)_{max}$
1.2
0.8
0.4
0
-0.4
-0.8
x
+ 0.55
○ 0.65
▼ 0.75
Ramp
← up →
Ramp
← down →
6
8
10
12
14
Time (sec)

FIG 13

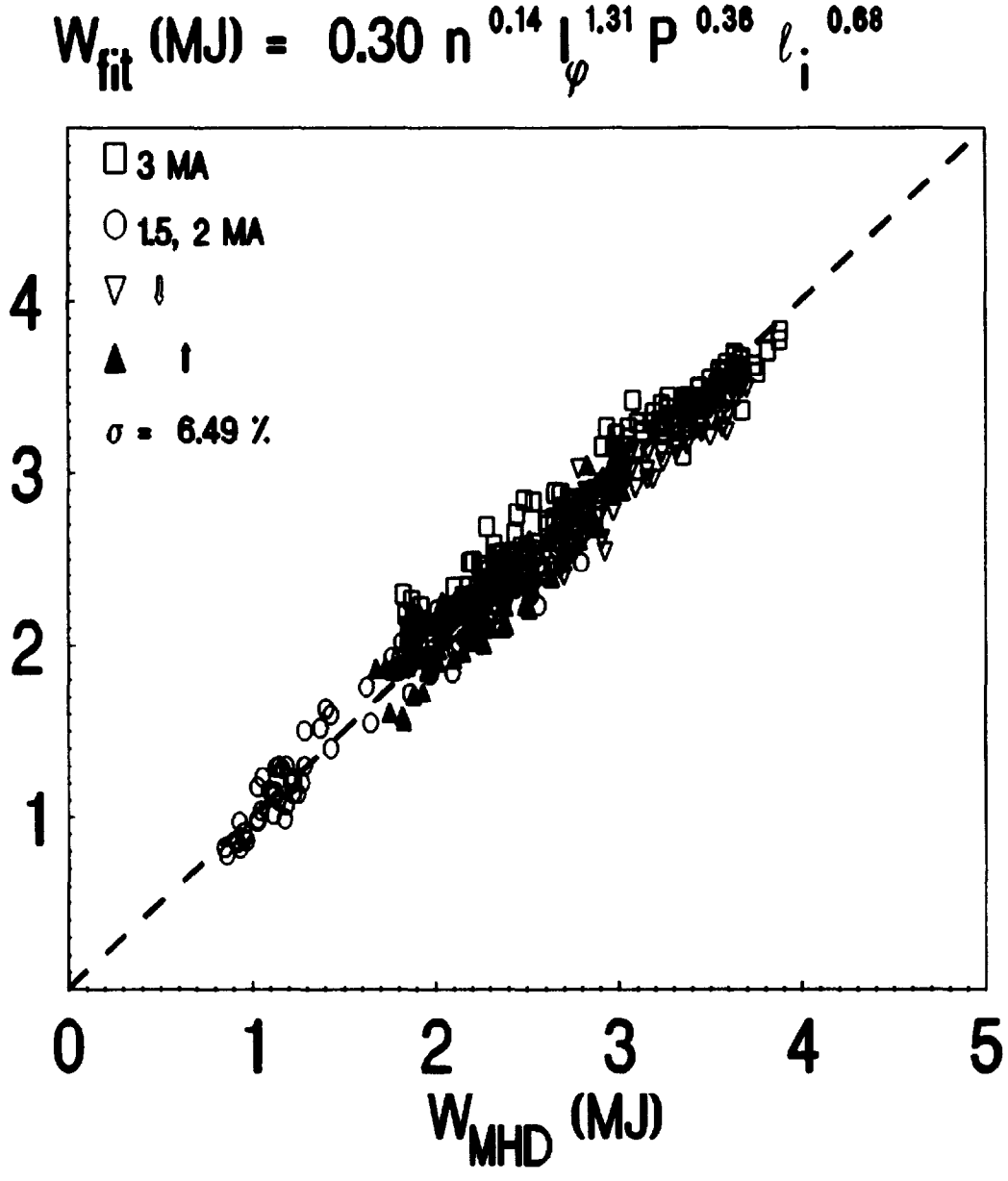
W_{fit} (MJ) = 0.30 n $^{0.14}$ I_φ $^{1.31}$ P $^{0.36}$ ℓ_i $^{0.68}$
3 MA
1.5, 2 MA
σ = 6.49 %
0
1
2
3
4
5
W_{MHD} (MJ)

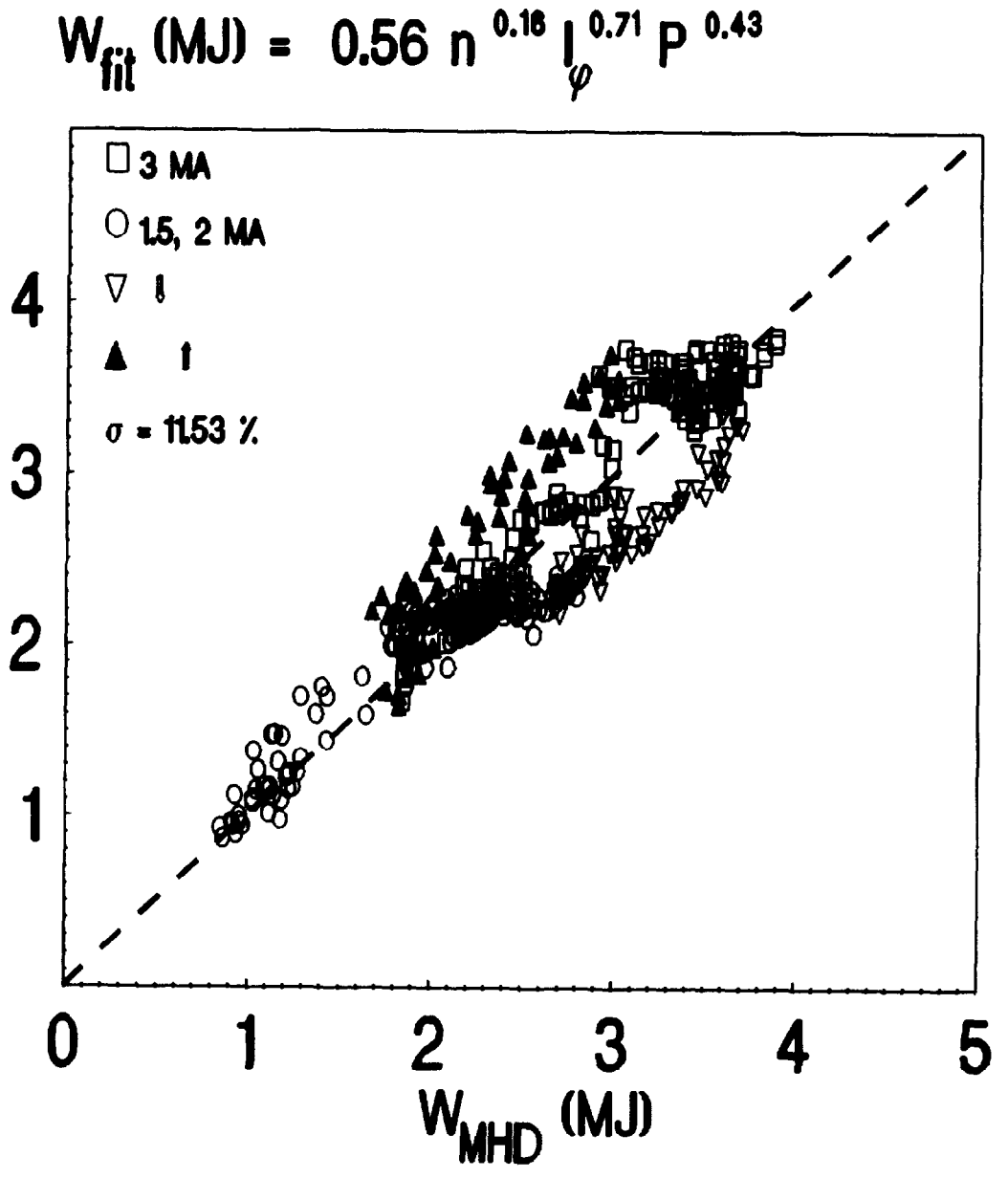
W_{fit} (MJ) = 0.56 n $^{0.16}$ I_φ $^{0.71}$ P $^{0.43}$
3 MA
1.5, 2 MA
σ = 11.53 %
0
1
2
3
4
5
W_{MHD} (MJ)

67%.

FIG 1

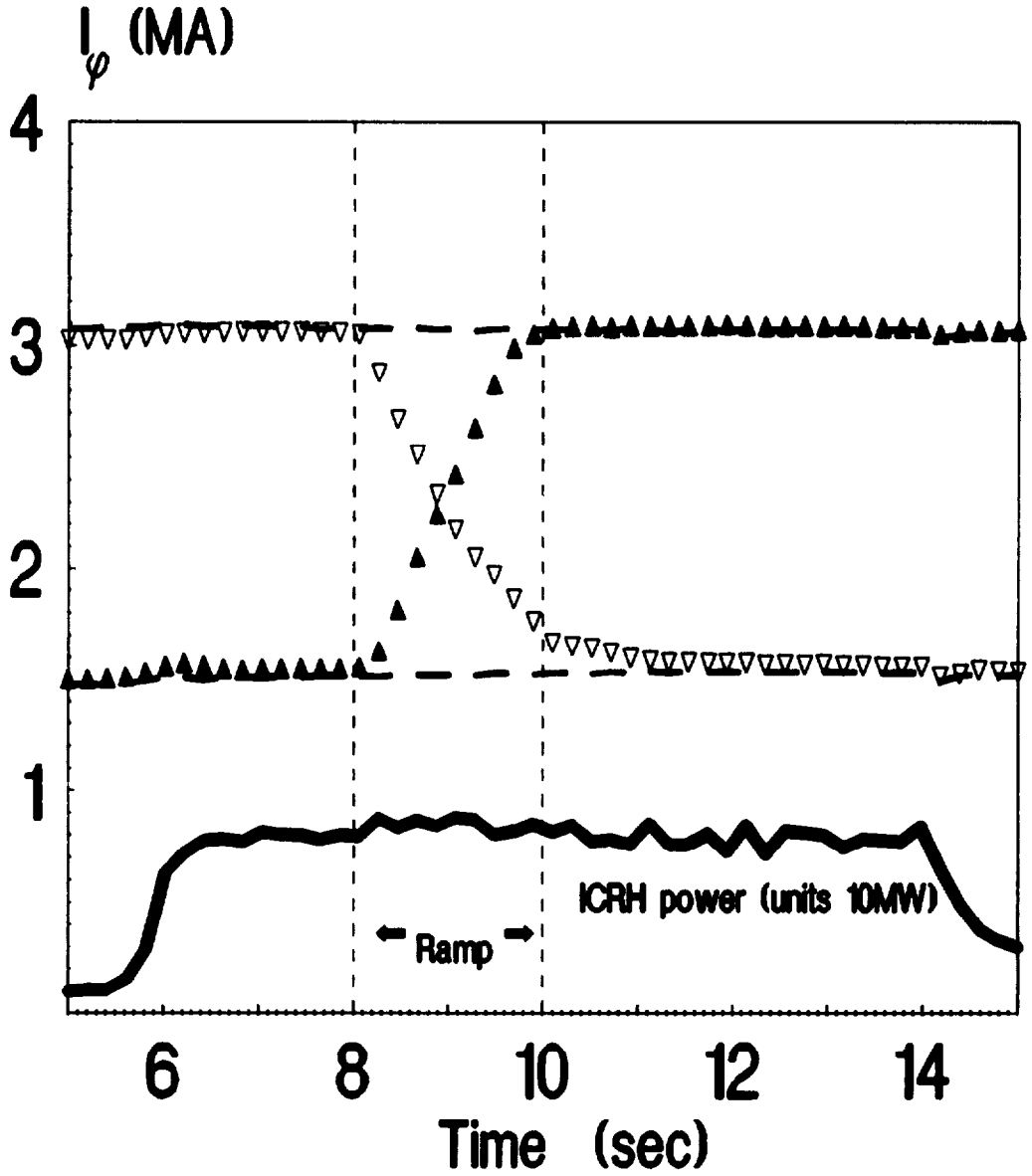
I_φ (MA)
4
3
2
1
ICRH power (units 10MW)
Ramp
6
8
10
12
14
Time (sec)

67%.

Fig 2

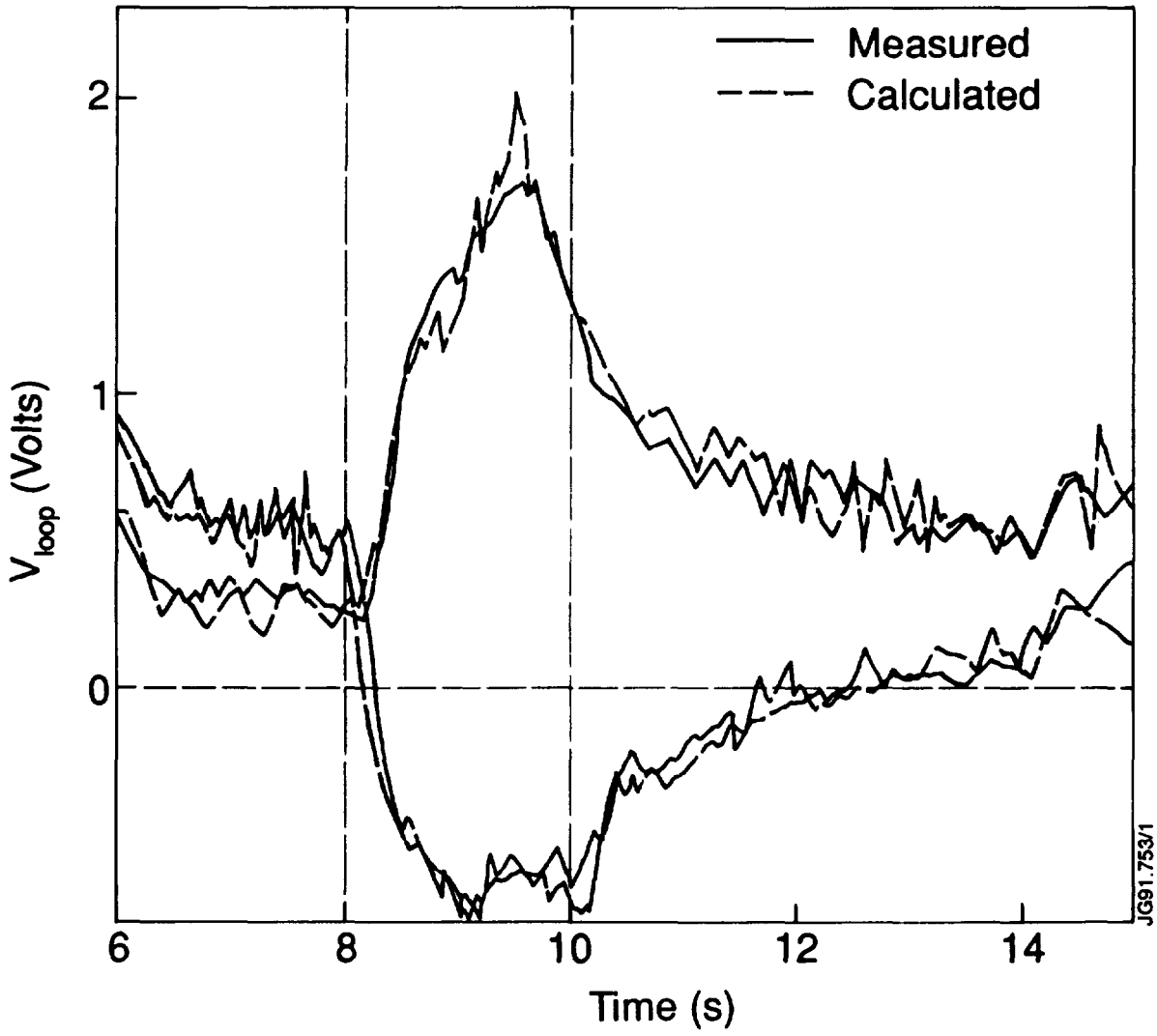
Measured
Calculated
2
1
0
V_{loop} (Volts)
6
8
10
12
14
Time (s)
JG91.753/1

67%
Fig 3

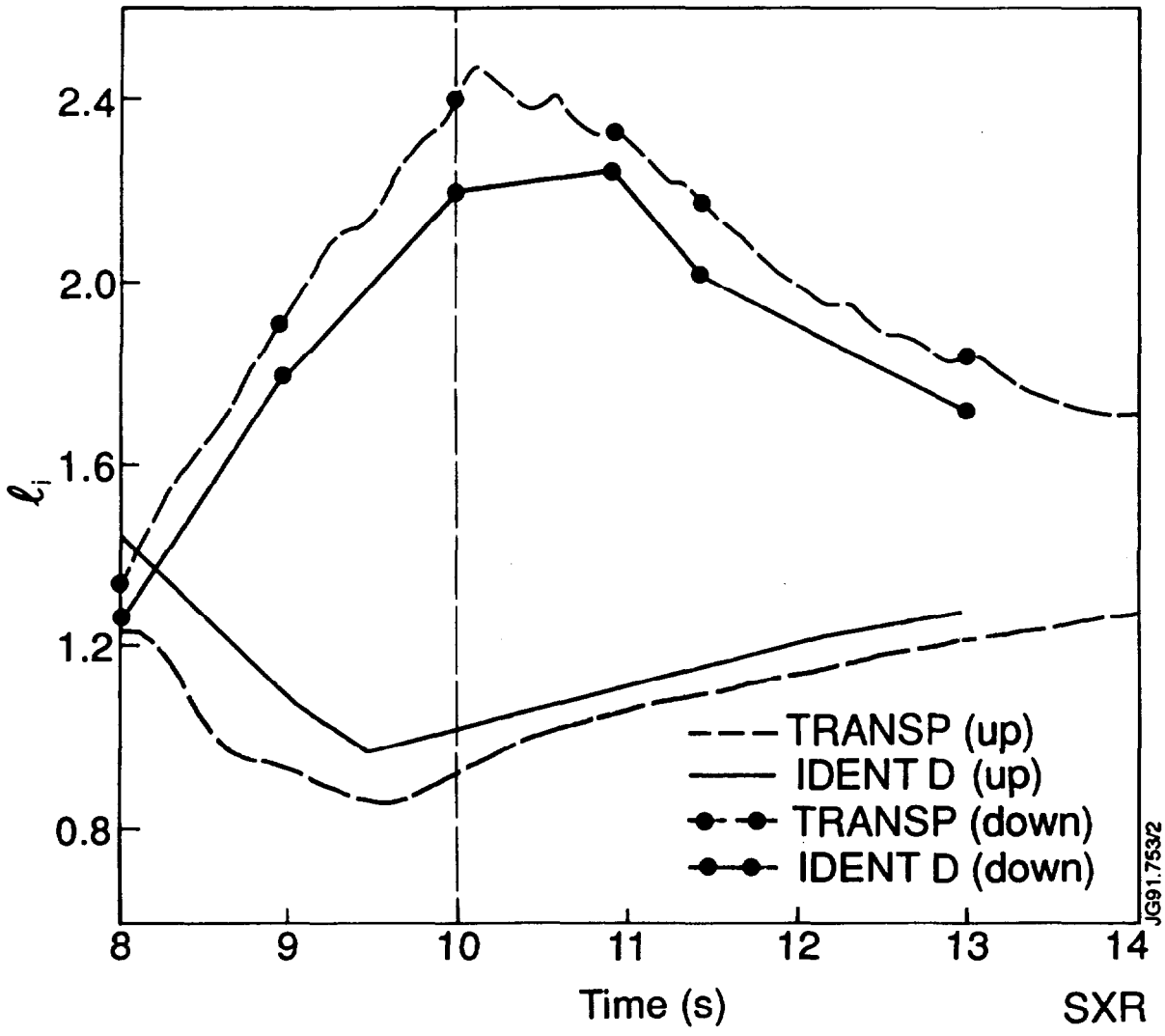
2.4
2.0
1.6
1.2
0.8
ℓ_i
8
9
10
11
12
13
14
Time (s)
TRANSP (up)
IDENT D (up)
TRANSP (down)
IDENT D (down)
SXR
JG91.753/2

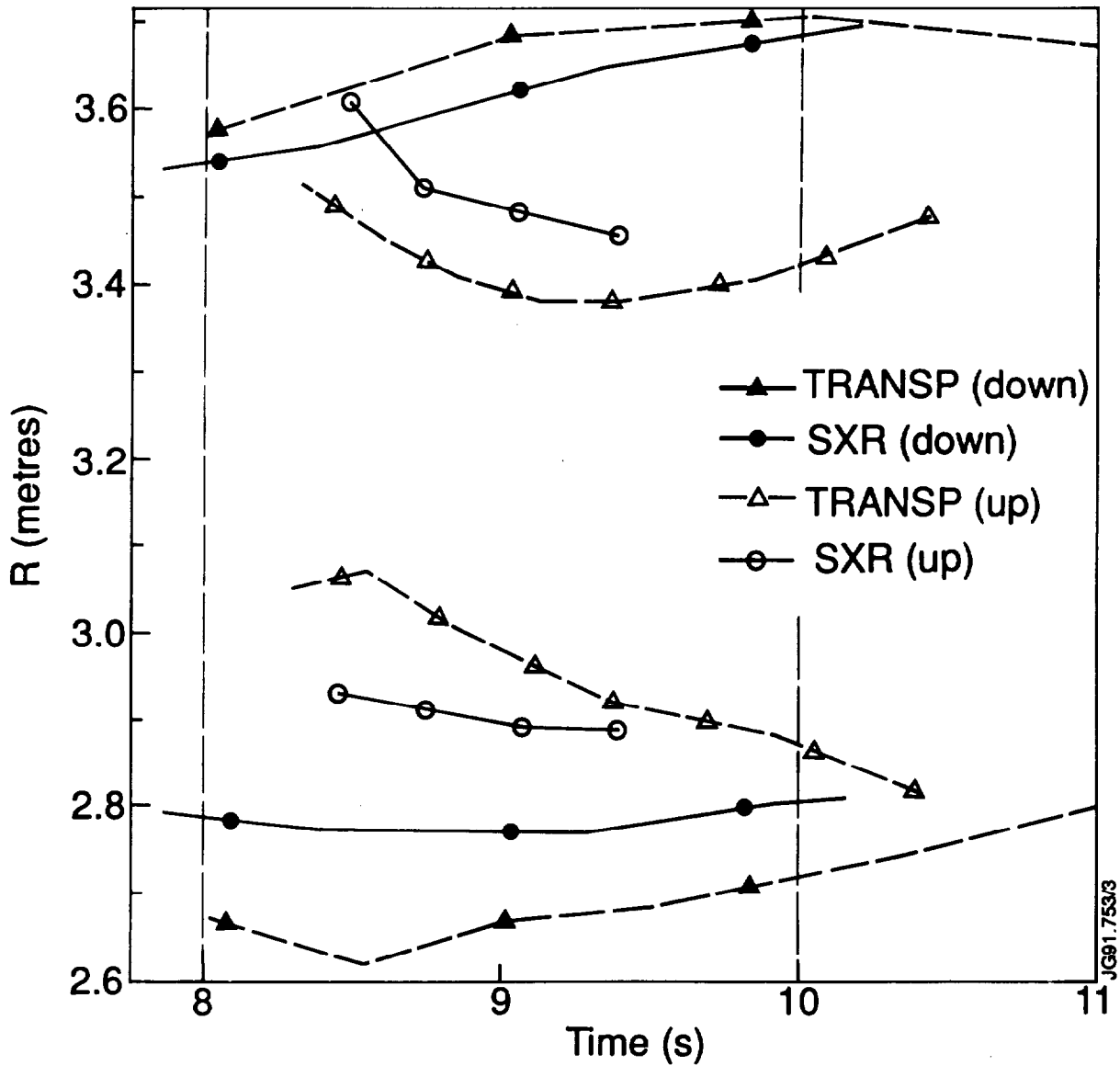
3.6
3.4
3.2
3.0
2.8
2.6
R (metres)
8
9
10
11
Time (s)
TRANSP (down)
SXR (down)
TRANSP (up)
SXR (up)
JG91.753/3

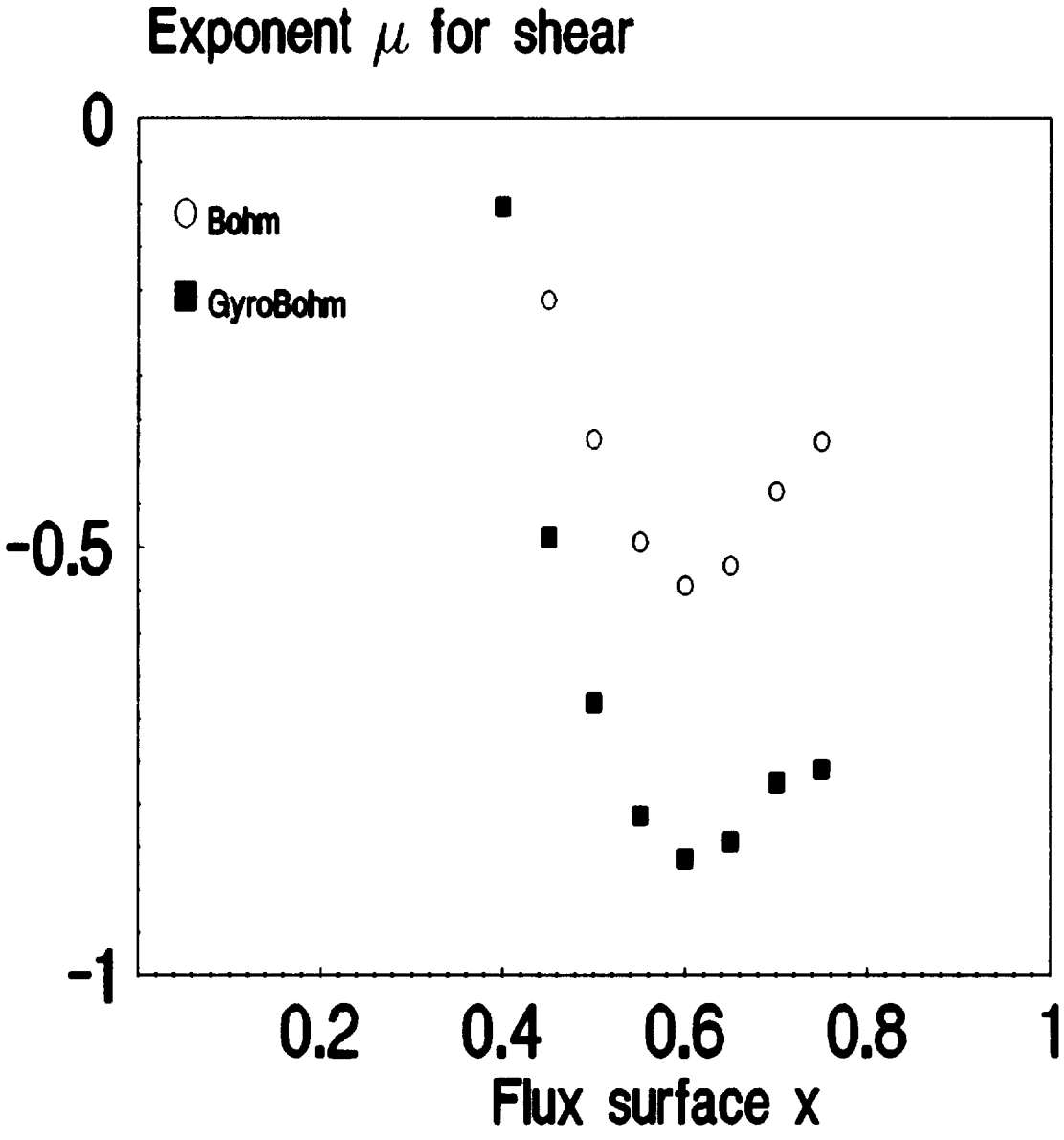
Exponent μ for shear
0
-0.5
-1
Bohm
GyroBohm
0.2
0.4
0.6
0.8
1
Flux surface x

67%
Fig 11

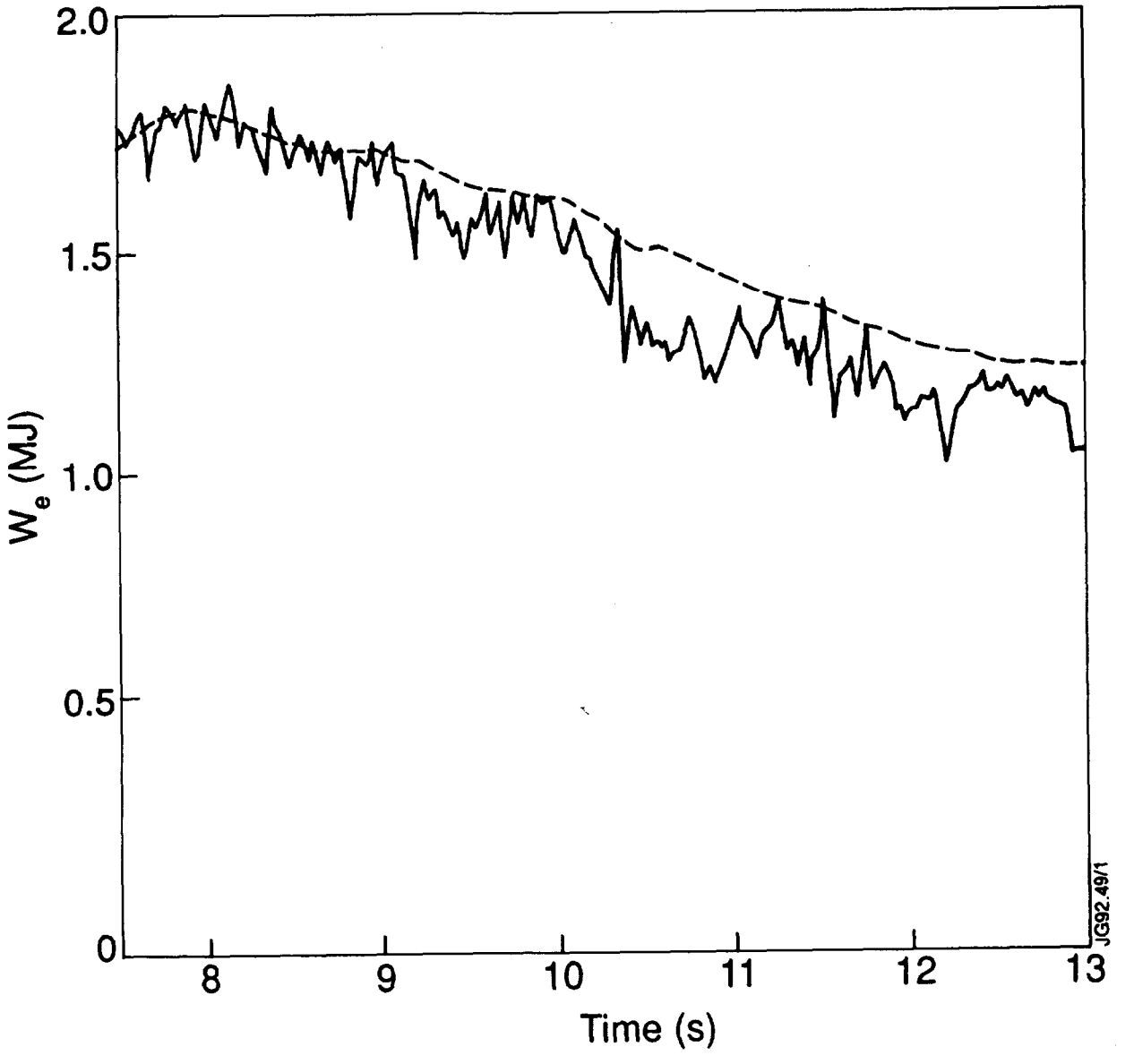

72%.
FIG 12 A

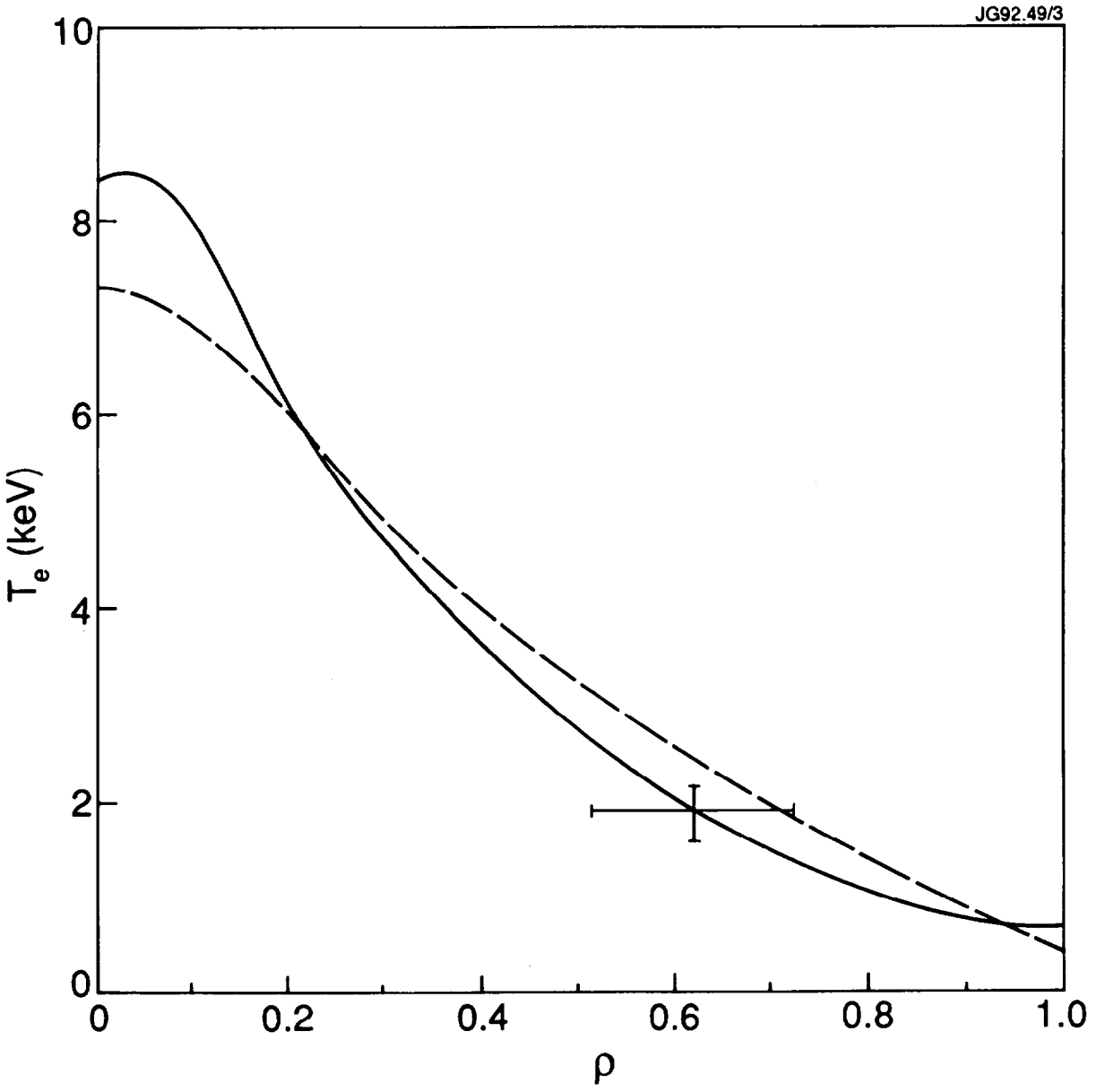

72%
FIG 12B

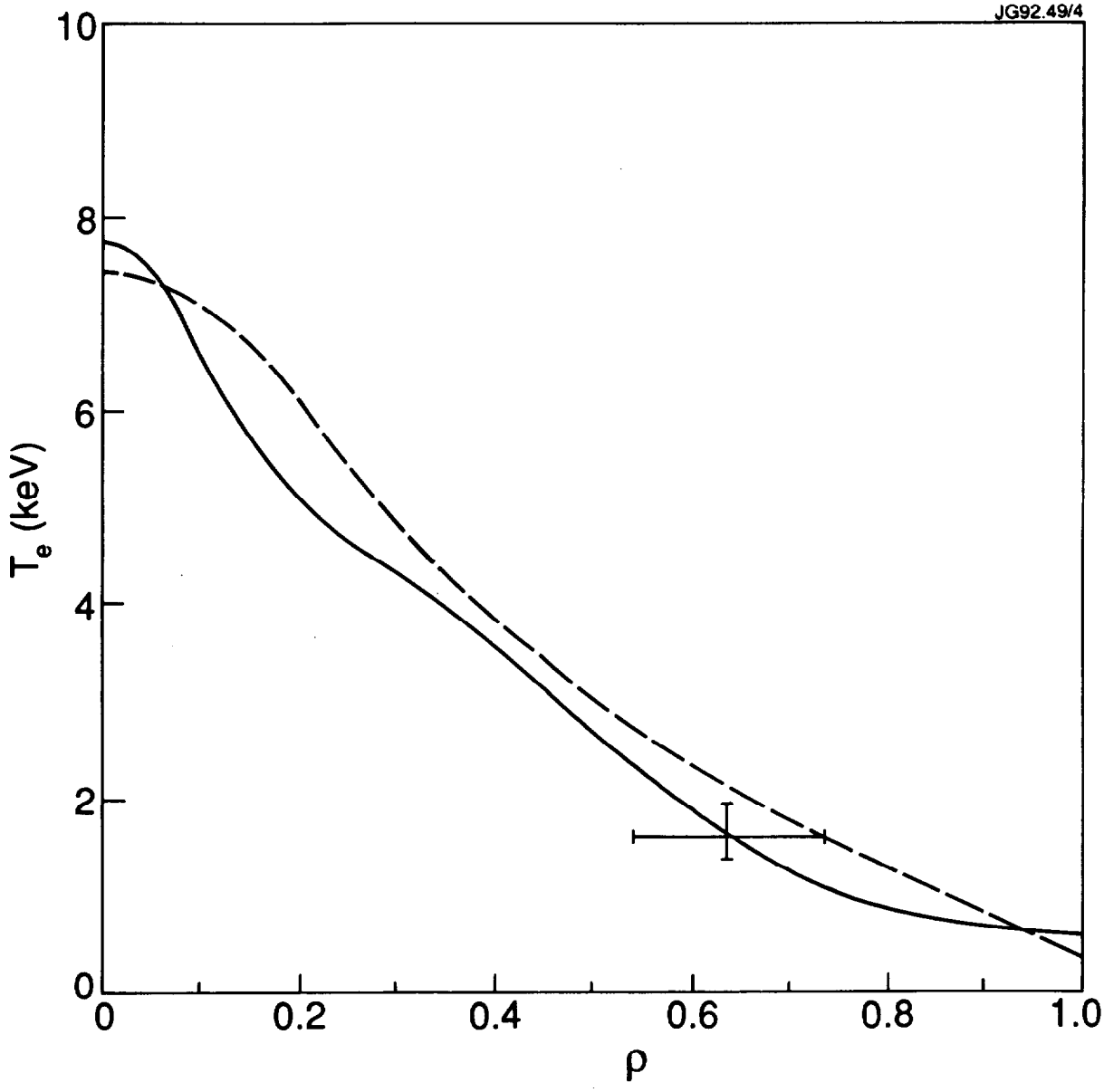

73%.
FIG 5B

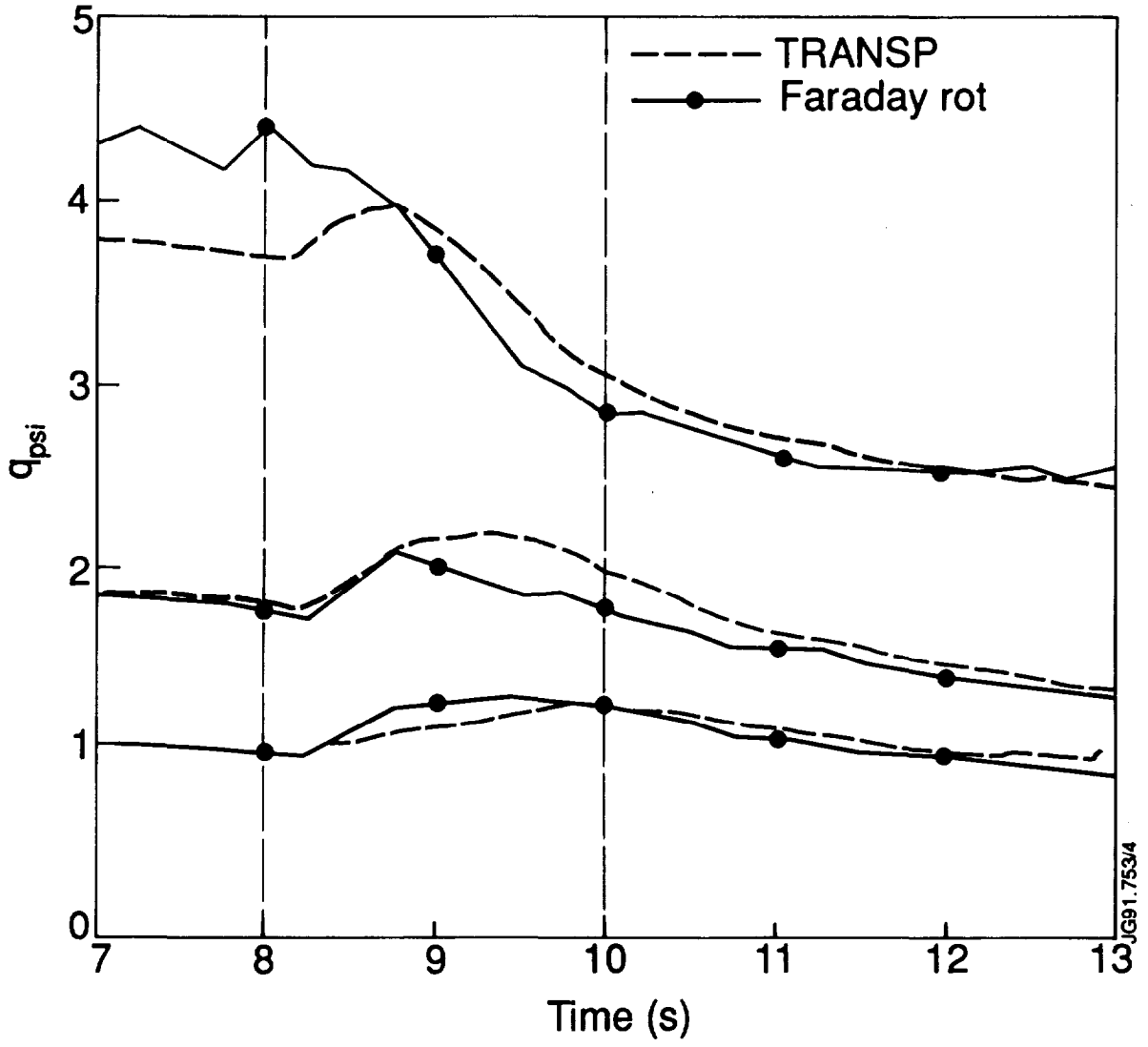
TRANSP
Faraday rot
q_{psi}
0
1
2
3
4
5
7
8
9
10
11
12
13
Time (s)
JG91.753/4

73%
FIG 5A.

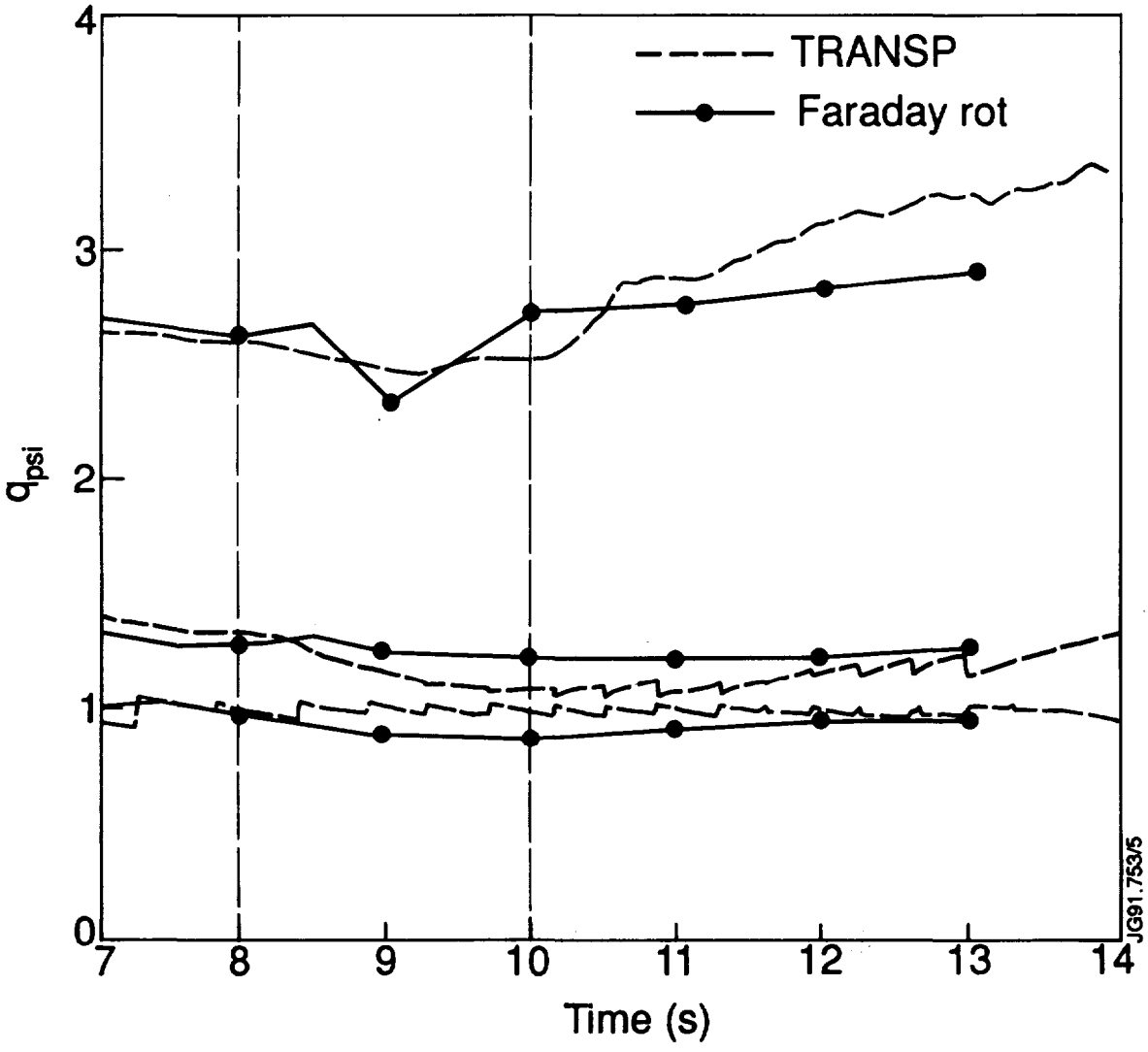
TRANSP
Faraday rot
q_{psi}
0
1
2
3
4
7
8
9
10
11
12
13
14
Time (s)
JG91.753/5

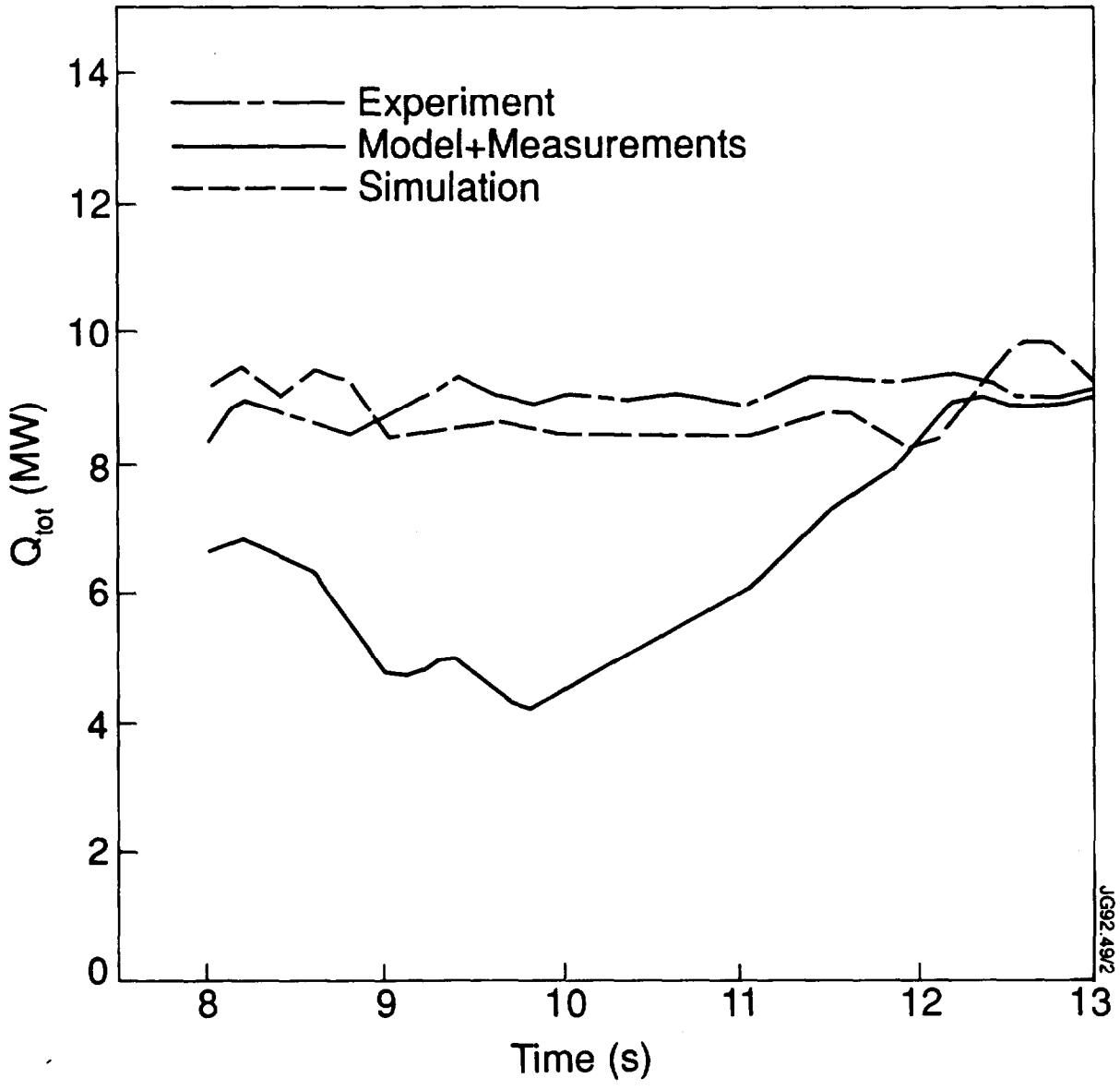
Experiment
Model+Measurements
Simulation
Q_{tot} (MW)
Time (s)
0
2
4
6
8
10
12
14
8
9
10
11
12
13
JG92.49/2

Fig 6

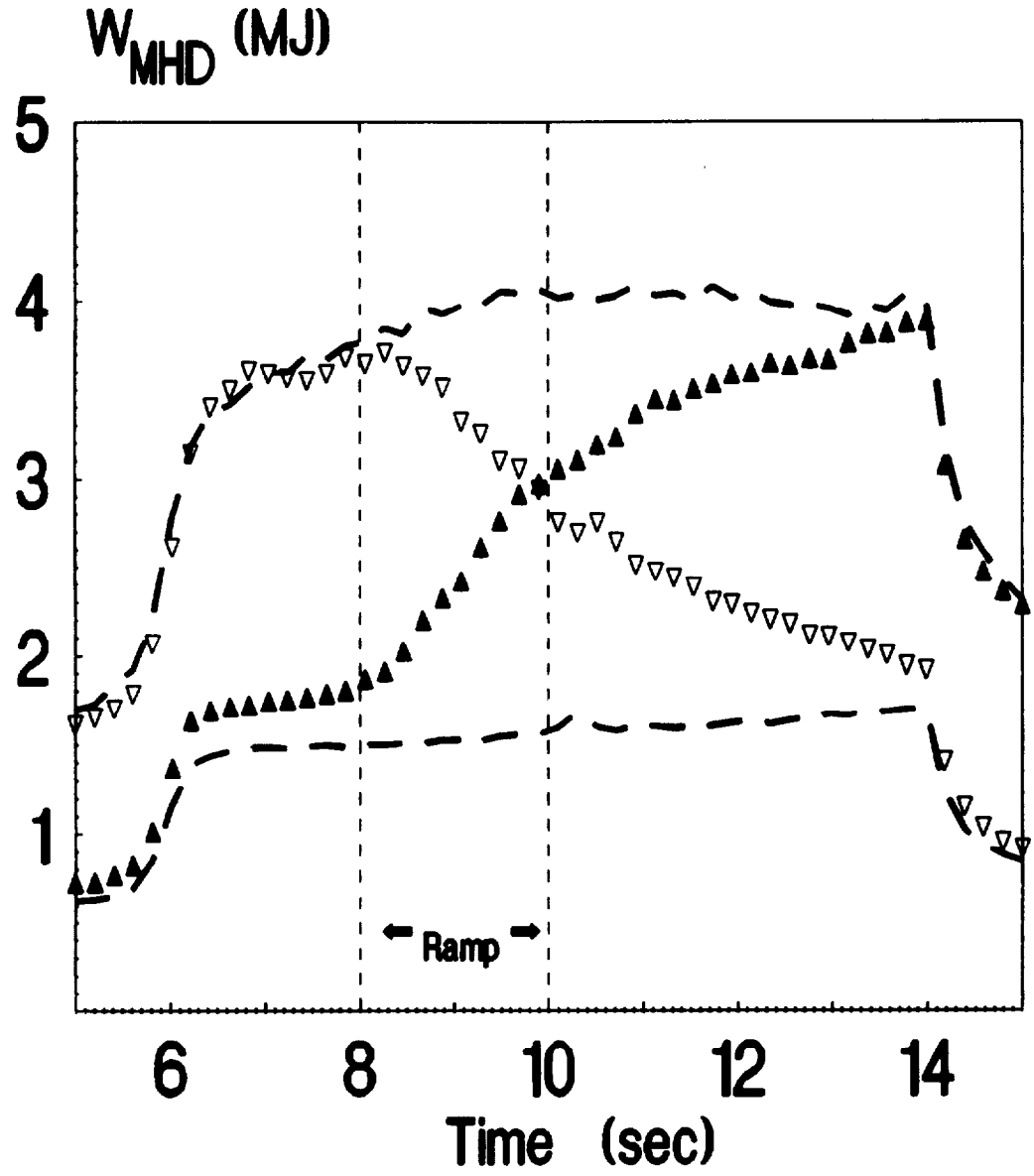

ANNEX

P.-H. REBUT, A. GIBSON, M. HUGUET, J.M. ADAMS[1], B. ALPER, H. ALTMANN, A. ANDERSEN[2], P. ANDREW[3], M. ANGELONE[4], S. ALI-ARSHAD, P. BAIGGER, W. BAILEY, B. BALET, P. BARABASCHI, P. BARKER, R. BARNSLEY[5], M. BARONIAN, D.V. BARTLETT, L. BAYLOR[6], A.C. BELL, G. BENALI, P. BERTOLDI, E. BERTOLINI, V. BHATNAGAR, A.J. BICKLEY, D. BINDER, H. BINDSLEV[2], T. BONICELLI, S.J. BOOTH, G. BOSIA, M. BOTMAN, D. BOUCHER, P. BOUCQUEY, P. BREGER, H. BRELEN, H. BRINKSCHULTE, D. BROOKS, A. BROWN, T. BROWN, M. BRUSATI, S. BRYAN, J. BRZOZOWSKI[7], R. BUCHSE[22], T. BUDD, M. BURES, T. BUSINARO, P. BUTCHER, H. BUTTGEREIT, C. CALDWELL-NICHOLS, D.J. CAMPBELL, P. CARD, G. CELENTANO, C.D. CHALLIS, A.V. CHANKIN[8], A. CHERUBINI, D. CHIRON, J. CHRISTIANSEN, P. CHUILON, R. CLAESEN, S. CLEMENT, E. CLIPSHAM, J.P. COAD, I.H. COFFEY[9], A. COLTON, M. COMISKEY[10], S. CONROY, M. COOKE, D. COOPER, S. COOPER, J.G. CORDEY, W. CORE, G. CORRIGAN, S. CORTI, A.E. COSTLEY, G. COTTRELL, M. COX[11], P. CRIPWELL[12], O. Da COSTA, J. DAVIES, N. DAVIES, H. de BLANK, H. de ESCH, L. de KOCK, E. DEKSNIS, F. DELVART, G.B. DENNE-HINNOV, G. DESCHAMPS, W.J. DICKSON[13], K.J. DIETZ, S.L. DMITRENKO, M. DMITRIEVA[14], J. DOBBING, A. DOGLIO, N. DOLGETTA, S.E. DORLING. P.G. DOYLE, D.F. DÜCHS, H. DUQUENOY, A. EDWARDS, J. EHRENBERG, A. EKEDAHL, T. ELEVANT[7], S.K. ERENTS[11], L.G. ERIKSSON, H. FAJEMIROKUN[12], H. FALTER, J. FREILING[15], F. FREVILLE, C. FROGER, P. FROISSARD, K. FULLARD, M. GADEBERG, A. GALETSAS, T. GALLAGHER, D. GAMBIER, M. GARRIBBA, P. GAZE, R. GIANNELLA, R.D. GILL, A GIRARD, A. GONDHALEKAR, D. GOODALL[11], C. GORMEZANO, N.A. GOTTARDI, C. GOWERS, B.J. GREEN, B. GRIEVSON, R. HAANGE, A. HAIGH, C.J. HANCOCK, P.J. HARBOUR, T. HARTRAMPF, N.C. HAWKES[11], P. HAYNES[11], J.L. HEMMERICH, T. HENDER[11], J. HOEKZEMA, D. HOLLAND, M. HONE, L. HORTON, J. HOW, M. HUART, I. HUGHES, T.P. HUGHES[10], M. HUGON, Y. HUO[16], K. IDA[17], B. INGRAM, M. IRVING, J. JACQUINOT, H. JAECKEL, J.F. JAEGER, G. JANESCHITZ, Z. JANKOVICZ[18], O.N. JARVIS, F. JENSEN, E.M. JONES, H.D. JONES, L.P.D.F. JONES, S. JONES[19], T.T.C. JONES, J.-F. JUNGER, F. JUNIQUE, A. KAYE, B.E. KEEN, M. KEILHACKER, G.J. KELLY, W. KERNER, A. KHUDOLEEV[21], R. KONIG, A. KONSTANTELLOS, M. KOVANEN[20], G. KRAMER[15], P. KUPSCHUS, R. LÄSSER, J.R. LAST, B. LAUNDY, L. LAURO-TARONI, M. LAVEYRY, K. LAWSON[11], M. LENNHOLM, J. LINGERTAT[22], R.N. LITUNOVSKI, A. LOARTE, R. LOBEL, P. LOMAS, M. LOUGHLIN, C. LOWRY, J. LUPO, A.C. MAAS[15], J. MACHUZAK[19], B. MACKLIN, G. MADDISON[11], C.F. MAGGI[23], G. MAGYAR, W. MANDL[22], V. MARCHESE, G. MARCON, F. MARCUS, J. MART, D. MARTIN, E. MARTIN, R. MARTIN-SOLIS[24], P. MASSMANN, G. MATTHEWS, H. McBRYAN, G. McCRACKEN[11], J. McKIVITT, P. MERIGUET, P. MIELE, A. MILLER, J. MILLS, S.F. MILLS, P. MILLWARD, P. MILVERTON, E. MINARDI[4], R. MOHANTI[25], P.L. MONDINO, D. MONTGOMERY[26], A. MONTVAI[27], P. MORGAN, H. MORSI, D. MUIR, G. MURPHY, R. MYRNÄS[28], F. NAVE[29], G. NEWBERT, M. NEWMAN, P. NIELSEN, P. NOLL, W. OBERT, D. O'BRIEN, J. ORCHARD, J. O'ROURKE, R. OSTROM, M. OTTAVIANI, M. PAIN, F. PAOLETTI, S. PAPASTERGIOU, W. PARSONS, D. PASINI, D. PATEL, A. PEACOCK, N. PEACOCK[11], R.J.M. PEARCE, D. PEARSON[12], J.F. PENG[16], R. PEPE DE SILVA, G. PERINIC, C. PERRY, M. PETROV[21], M.A. PICK, J. PLANCOULAINE, J.-P POFFÉ, R. PÖHLCHEN, F. PORCELLI, L. PORTE[13], R. PRENTICE, S. PUPPIN, S. PUTVINSKII[8], G. RADFORD[30], T. RAIMONDI, M.C. RAMOS DE ANDRADE, R. REICHLE, J. REID, S. RICHARDS, E. RIGHI, F. RIMINI, D. ROBINSON[11], A. ROLFE, R.T. ROSS, L. ROSSI, R. RUSS, P. RUTTER, H.C. SACK, G. SADLER, G. SAIBENE, J.L. SALANAVE, G. SANAZZARO, A. SANTAGIUSTINA, R. SARTORI, C. SBORCHIA, P. SCHILD, M. SCHMID, G. SCHMIDT[31], B. SCHUNKE, S.M. SCOTT, L. SERIO, A SIBLEY, R. SIMONINI, A.C.C. SIPS, P. SMEULDERS, R. SMITH, R. STAGG, M. STAMP, P. STANGEBY[3], R. STANKIEWICZ[32], D.F. START, C.A. STEED, D. STORK, P.E. STOTT, P. STUBBERFIELD, D. SUMMERS, H. SUMMERS[13], L. SVENSSON, J.A. TAGLE[33], M. TALBOT, A. TANGA, A. TARONI, C. TERELLA, A TERRINGTON, A TESINI, P.R. THOMAS, E. THOMPSON, K. THOMSEN, F. TIBONE, A. TISCORNIA, P. TREVALION, B. TUBBING, P. VAN BELLE, H. VAN DER BEKEN, G. VLASES, M. VON HELLERMANN, T. WADE, C. WALKER, R. WALTON[31], D. WARD, M.L. WATKINS, N. WATKINS, M.J. WATSON, S. WEBER[34], J. WESSON, T.J. WIJNANDS, J. WILKS, D. WILSON, T. WINKEL, R. WOLF, D. WONG, C. WOODWARD, Y. WU[35], M. WYKES, D. YOUNG, I.D. YOUNG, L. ZANNELLI, A. ZOLFAGHARI[19], W. ZWINGMANN

[1] Harwell Laboratory, UKAEA, Harwell, Didcot, Oxfordshire, UK.
[2] Risø National Laboratory, Roskilde, Denmark.
[3] Institute for Aerospace Studies, University of Toronto, Downsview, Ontario, Canada.
[4] ENEA Frascati Energy Research Centre, Frascati, Rome, Italy.
[5] University of Leicester, Leicester, UK.
[6] Oak Ridge National Laboratory, Oak Ridge, TN, USA.
[7] Royal Institute of Technology, Stockholm, Sweden.
[8] I.V. Kurchatov Institute of Atomic Energy, Moscow, Russian Federation.
[9] Queens University, Belfast, UK.
[10] University of Essex, Colchester, UK.
[11] Culham Laboratory, UKAEA, Abingdon, Oxfordshire, UK.
[12] Imperial College of Science, Technology and Medicine, University of London, London, UK.
[13] University of Strathclyde, Glasgow, UK.
[14] Keldysh Institute of Applied Mathematics, Moscow, Russian Federation.
[15] FOM-Institute for Plasma Physics "Rijnhuizen", Nieuwegein, Netherlands.
[16] Institute of Plasma Physics, Academia Sinica, Hefei, Anhui Province, China.
[17] National Institute for Fusion Science, Nagoya, Japan.
[18] Soltan Institute for Nuclear Studies, Otwock/Świerk, Poland.
[19] Plasma Fusion Center, Massachusetts Institute of Technology, Boston, MA, USA.
[20] Nuclear Engineering Laboratory, Lappeenranta University, Finland.
[21] A.F. Ioffe Physico-Technical Institute, St. Petersburg, Russian Federation.
[22] Max-Planck-Institut für Plasmaphysik, Garching, Germany.
[23] Department of Physics, University of Milan, Milan, Italy.
[24] Universidad Complutense de Madrid, Madrid, Spain.
[25] North Carolina State University, Raleigh, NC, USA.
[26] Dartmouth College, Hanover, NH, USA.
[27] Central Research Institute for Physics, Budapest, Hungary.
[28] University of Lund, Lund, Sweden.
[29] Laboratorio Nacional de Engenharia e Tecnologia Industrial, Sacavem, Portugal.
[30] Institute of Mathematics, University of Oxford, Oxford, UK.
[31] Princeton Plasma Physics Laboratory, Princeton University, Princeton, NJ, USA.
[32] RCC Cyfronet, Otwock/Świerk, Poland,
[33] Centro de Investigaciones Energéticas, Medioambientales y Tecnológicas, Madrid, Spain.
[34] Freie Universität, Berlin, Germany.
[35] Insitute for Mechanics, Academia Sinica, Beijing, China.